

Photoelectron Circular Dichroism of Aqueous-Phase Alanine

Dominik Stemer,^{*,†} Stephan Thürmer,^{*,‡} Florian Trinter,[†] Uwe Hergenhahn,[†]
Michele Pugini,[†] Bruno Credidio,[†] Sebastian Malerz,[¶] Iain Wilkinson,[§]
Laurent Nahon,^{||} Gerard Meijer,[†] Ivan Powis,[⊥] and Bernd Winter^{*,†}

[†]*Fritz-Haber-Institut der Max-Planck-Gesellschaft, Berlin 14195, Germany.*

[‡]*Department of Chemistry, Kyoto University, Kyoto 606-8502, Japan.*

[¶]*Department of Optics and Beamlines, Helmholtz-Zentrum Berlin für Materialien und
Energie, Berlin 14109, Germany.*

[§]*Institute for Electronic Structure Dynamics, Helmholtz-Zentrum Berlin für Materialien
und Energie, Berlin 14109, Germany.*

^{||}*Synchrotron SOLEIL, St. Aubin 91190, France.*

[⊥]*School of Chemistry, The University of Nottingham, Nottingham NG7 2RD, UK.*

E-mail: dstemer@fhi-berlin.mpg.de; thuermer@kuchem.kyoto-u.ac.jp; winter@fhi-berlin.mpg.de

Abstract

Amino acids and other small chiral molecules play key roles in biochemistry. However, in order to understand how these molecules behave in vivo, it is necessary to study them under aqueous-phase conditions. Photoelectron circular dichroism (PECD) has emerged as an extremely sensitive probe of chiral molecules, but its suitability for application to aqueous solutions had not yet been proven. Here, we report on our PECD measurements of aqueous-phase alanine, the simplest chiral amino acid. We demonstrate that the PECD response of alanine in water is different for each of alanine's

carbon atoms, and is sensitive to molecular structure changes (protonation states) related to the solution pH. For C 1s photoionization of alanine’s carboxylic acid group, we report PECD of comparable magnitude to that observed in valence-band photoelectron spectroscopy of gas-phase alanine. We identify key differences between PECD experiments from liquids and gases, discuss how PECD may provide information regarding solution-specific phenomena — for example the nature and chirality of the solvation shell surrounding chiral molecules in water — and highlight liquid-phase PECD as a powerful new tool for the study of aqueous-phase chiral molecules of biological relevance.

Introduction

Chirality describes a broad class of objects that share the property of being non-superposable with their mirror images. This general property of chirality may be found at all size scales and levels of complexity in nature, from human hands and sea shells down to small molecules. Many of the molecules most essential for life on Earth are chiral, including macromolecules such as proteins and DNA as well as smaller building blocks of life such as amino acids and sugars. All chiral biomolecules have been found to be overwhelmingly present in only a single enantiomeric form in living organisms, despite the mirror-image enantiomeric forms of a chiral molecule exhibiting identical physical and chemical properties in achiral environments (exempting small anticipated energetic differences between enantiomers due to parity-violating effects in the weak interactions).¹ The origins of this asymmetry in biology remain unresolved. In chiral environments, the chemical activity of the different enantiomers of a chiral molecule can differ dramatically. As such, experimental methods capable of distinguishing between enantiomers under biologically relevant conditions are of direct interest for chemical and life sciences. Absorption-based electronic circular dichroism (ECD) describes the asymmetry in absorption of left- or right-handed circularly polarized light (CPL) in the UV-visible range by different enantiomers of a chiral molecule. ECD is widely used as a means to determine the degree of enantiomeric excess for chiral molecules in solution.²

However, it is dependent on the interaction between the electric and magnetic dipoles of the chiral system with the CPL, and correspondingly the intrinsic effect magnitudes are small, generally on the order of 0.01%.³

In 2001, it was first experimentally demonstrated that one-photon photoionization of chiral molecules by circularly polarized synchrotron radiation may also be used to differentiate between enantiomers.⁴ This photoelectron circular dichroism (PECD) — predicted theoretically 25 years earlier by Ritchie^{5,6} — manifests as a forward-backward asymmetry in the measured photoelectron flux along an experimental axis defined by the direction of light propagation. Arising purely due to electric-dipole interactions, PECD is much more pronounced than ECD, exhibiting asymmetries on the order of 1% up to a few 10's% for randomly oriented molecules.⁷ Alignment of molecules has been demonstrated to further increase PECD effect sizes.⁸⁻¹⁰ PECD appears to be a general feature in photoionization of chiral systems by CPL, having been observed in core-level and valence-band photoemission from terpenes¹¹⁻¹⁴ as well as from molecular dimers and larger clusters,^{15,16} amino acids,¹⁷⁻¹⁹ organometallic complexes,²⁰ and nanoparticles.¹⁸ In addition to the traditional strengths of photoelectron spectroscopy, including chemical-state and site specificity, PECD is uniquely sensitive to small differences in molecular electronic structure and is capable of clearly distinguishing between different structural and conformational isomers of a chiral molecule.^{21,22} PECD is a powerful method capable of much more than the resolution of enantiomers and the determination of enantiomeric excess. These very appealing analytical capabilities have driven the growing field of laser-based multi-photon PECD since 2012.²³⁻²⁵

Water is critically important for biochemistry, playing an active role in determining the functionality of amino acids, proteins, and DNA through structure stabilization and mediation of intra- and intermolecular interactions.²⁶ For chiral molecules in solution, interactions with solvent molecules, even achiral solvents such as water, may profoundly influence both the magnitude and the sign of measured chiroptical effects.²⁷ Additionally, it is possible that achiral solvent molecules may themselves adopt chiral arrangements within the first solva-

tion shell around a chiral solute, mimicking to some extent the solute’s chiral structure.²⁸ Understanding the complex interactions between chiral solutes and achiral solvents is clearly a necessary prerequisite for developing deeper insight into the chemical activity of chiral molecules in solution, whether in biochemical or synthetic contexts. Core-level PECD seems uniquely suited for an investigation into the remarkably active role of solvent molecules in determining chiral solute properties. However, PECD of liquid-phase samples has only very recently become experimentally feasible.^{29,30}

The development and growth of liquid-jet photoelectron spectroscopy (LJ-PES) over the past few decades has led to the solution of many of the technical obstacles that long prohibited the study of volatile liquids under the vacuum conditions required for PES.^{31,32} However, the application of PECD to liquids, and particularly to aqueous solutions, introduces a number of new experimental challenges that are not present for gas-phase studies. PECD, based upon the scattering and interference of departing partial electron waves, exhibits a strong kinetic-energy dependence, with the most pronounced effects manifesting for photoelectrons with kinetic energy of less than approximately 15 eV.¹¹ For photoelectron spectroscopy of condensed-phase systems this poses a clear challenge due to the unavoidable convolution of primary photoelectron spectral features in this kinetic-energy range with the high-intensity low-energy electron background composed of electrons inelastically scattered in the sample bulk. For the cases of liquid water and of bulk-soluble species in aqueous solution, the opening of efficient quasi-elastic scattering channels within the same kinetic-energy range additionally leads to the broadening of photoelectron features and the homogenization of photoelectron angular distributions.^{33,34}

Despite these challenges, we have previously demonstrated the viability of liquid-phase PECD measurements for the chiral molecule fenchone as a neat liquid.³⁰ We now report PECD in core-level photoionization of aqueous-phase alanine — the simplest chiral amino acid — at different solution pH values corresponding to the cationic, zwitterionic, and anionic form of the molecule. We summarize the results of our measurements, highlight the

key differences in measuring PECD in the aqueous and gas phases, and discuss the potential influence of water solvation on PECD. We outline new opportunities for aqueous-phase PECD going forward, including the relatively straightforward application of PECD to study cationic or anionic chiral molecules; a topic that has only recently begun to be explored.^{35–37} More generally, this study constitutes the first core-level PECD investigation of chiral amino acids in any context. Liquid-phase PECD studies of the elementary constituents of life are highly relevant to *in vivo* biological conditions. We present a first step toward a bottom-up approach to understanding biomolecular complexity through the preparation of simple aqueous solutions, enabling the study of fragile thermolabile chiral species such as amino acids, peptides, sugars, and nucleic acids, whose vaporization into the gas phase is extremely challenging.

Experimental Considerations

In this work, we focus on core-level C 1s measurements of aqueous-phase alanine. Alanine has three chemically distinct carbon atoms — a carboxylic acid group, a chiral central carbon adjacent to an amine group, and a methyl group, which we denote C₁, C₂, and C₃, respectively — resulting in a solution-phase C 1s PE spectrum with three distinct features that overlap to varying degrees depending on the solution pH / alanine protonation state (Fig. 1). An investigation of the precisely energy-referenced C 1s spectrum of alanine is not the focus of this work, and we have aligned all spectra discussed below to the C₃ peak position (corresponding the alanine’s methyl group, see gray dashed line in Fig. 1) in order to better illustrate the kinetic-energy (KE) shifts occurring for C₁ and C₂ upon protonation or deprotonation. As we did not employ the energy-referencing scheme outlined in our earlier work,^{38–40} the KE axes presented in this work represent as-measured values. These values may be subject to inaccuracies due to spectrometer offsets, the presence of streaming potentials and other stray fields, and changes in the bulk electronic structure of water upon the addition of large amounts of NaOH and HCl needed for pH adjustment.^{41–43}

To track chemical shifts upon protonation / deprotonation of alanine’s functional groups, we first measured PE spectra from aqueous-phase alanine for solution pH values of 1, 7, and 13 using 335 eV photons, thereby generating photoelectrons with approximately 40–45 eV KE. These pH values were chosen based on the pKa values of alanine’s functional groups (2.3 and 9.9 for alanine’s carboxylic acid and amine groups in water, respectively) and ensured that, for a given solution pH, >95% (>99% for pH 7 and 13) of the alanine molecules in solution adopted a single charge state. At these rather high KEs the primary PE features are well separated from the high-intensity background region mentioned above, which becomes significant below approximately 20 eV KE.

Under strongly acidic conditions, alanine is predominantly in a cationic state (Ala^+), with the amine functional group protonated (Fig. 1, top). In this state, despite some overlap between C_2 and C_3 , the three carbon PE features are easily resolvable owing to pronounced chemical shifts arising due to the different chemical environments of the carbon sites. The lowest KE feature corresponds to photoelectrons originating from the relatively electronegative COOH group (C_1). The central PE feature corresponds to the chiral center adjacent to the amine group (C_2), and the final feature is attributable to the methyl group (C_3). These assignments are consistent with previous solid-state and gas-phase work.^{44,45} As can be seen by comparing the pH 1 and pH 7 data in Figure 1, deprotonation of the carboxylic acid for zwitterionic Ala^{zw} is accompanied by a noticeable chemical shift of the C_1 peak (relative to the C_3 peak) of approximately 0.71 eV toward higher KE (lower binding energy), reflecting the increasing electron density at that site upon deprotonation. In contrast, C_2 does not experience much of a chemical shift, suggesting that the central carbon is not particularly sensitive to the changing electron density on the neighboring functional group. This may be a consequence of effective charge screening by nearby water molecules.⁴⁶ At this pH, all three primary PE features are still easily resolvable. At pH 13, alanine is found in the anionic form, Ala^- , with the carboxylic acid deprotonated and the amine group neutral. In this case, we observe a chemical shift of 0.44 eV toward lower KE for the C_2 peak, corresponding

to an increase in electron density at that group compared to the pH 7 case. This chemical shift results in substantial overlap of the C₂ and C₃ peaks. We note that the C₁ peak remains clearly isolated from the C₂ and C₃ features for all charge states, thereby simplifying the determination of PECD for this carbon site.

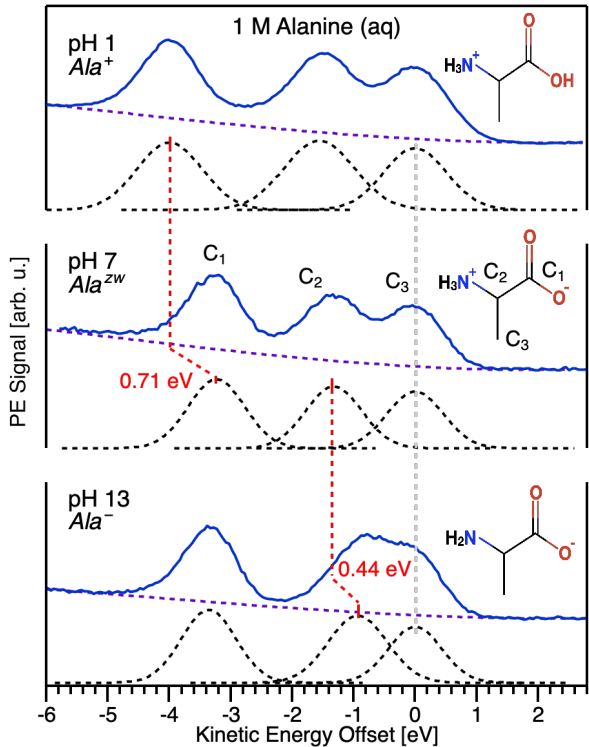


Figure 1: Representative as-measured C 1s photoelectron spectra corresponding to aqueous-phase alanine’s three chemically distinct carbons measured with $h\nu = 335$ eV photons under acidic (top), neutral (middle), and basic (bottom) aqueous conditions. Measurements were conducted with 1 M aqueous solutions of L-alanine. The dashed black curves are fits to the data following the subtraction of background signals (dashed purple lines) using Gaussian profiles, with the widths of the overlapping C₂ and C₃ peaks constrained to differ by a maximum of 10%. All spectra were shifted to the as-measured kinetic energy of the C₃ peak, corresponding to the methyl group (dashed gray vertical line). Molecular structures of the dominant protonation state of alanine at the various pH values investigated are shown as insets.

Similarly to our previous study of PECD from neat liquid fenchone,³⁰ we determined PECD using synchrotron radiation and an in-vacuum liquid-jet photoemission spectrometer via sequential measurements of photoelectron flux upon photoionization of aqueous alanine

solutions with left- and right-handed CPL (see Experimental section below for additional details). The implemented beamline settings corresponding to each type of polarization were confirmed previously through measurements of PECD from gaseous fenchone.^{29,30} Electrons were detected in the backward direction, with our electron analyzer mounted at $\approx 50^\circ$ with respect to the axis of light propagation, approximating a magic-angle geometry of 54.74° .²⁹ This angle was chosen due to technical considerations of compatibility with the open port at the P04 soft x-ray beamline, where these measurements were performed.

For single-photon photoionization of a randomly oriented sample,⁴⁷ the normalized photoelectron angular distribution (PAD) within the electric-dipole approximation is given by:

$$I^p(\theta) = 1 + b_1^p P_1(\cos\theta) + b_2^p P_2(\cos\theta) \quad (1)$$

Here, $I^p(\theta)$ is the photoionization intensity at an angle θ measured with respect to the photon-propagation direction for a given light polarization ($p = \pm 1$ for circularly polarized light and 0 for linearly polarized light, respectively). P_n represents the Legendre polynomial of the n th order. The two coefficients b_1^p and b_2^p completely encompass the target-specific contribution to the PAD under a fixed set of experimental conditions. For achiral molecules, $b_1^p = 0$ and thus the PAD is described by b_2^p , more commonly denoted β for experiments involving linearly polarized light (i.e. $b_2^0 = \beta$, while $b_2^{\pm 1} = -\beta/2$).⁴⁸ For chiral molecules, $b_1^{\pm 1}$ may be non-zero and $b_1^{+1} = -b_1^{-1}$, changing sign upon inversion of the handedness of CPL (or of the enantiomer). An asymmetry factor, G , may be defined as the simple difference between left- and right-handed PE intensities divided by their average. Using Eq. 1 and noting that $P_1(x) = x$, we then have:

$$G = \frac{I^{+1}(\theta) - I^{-1}(\theta)}{[I^{+1}(\theta) + I^{-1}(\theta)]/2} = \frac{2b_1^{+1}\cos\theta}{1 + b_2^{\pm 1}P_2(\cos\theta)} \quad (2)$$

It can be seen that this provides a means to extract $b_1^{\pm 1}$ although, in general, a knowledge of $b_2^{\pm 1}$ is also necessary. However, $P_2(\cos(54.74^\circ)) = 0$. Thus, at magic angle:

$$b_1^{+1} = \pm \frac{[I^{+1} - I^{-1}]}{[I^{+1} + I^{-1}]} \cdot \frac{1}{\cos(54.74^\circ)}, \quad (3)$$

the negative sign applying when, as here, measurement is made in the backwards hemisphere. We note that $P_2(\cos(50^\circ)) \neq 0$, and we discuss the relevant consequences of our near magic-angle measurement geometry in greater detail below.

As b_1^{+1} simply changes sign upon exchange of enantiomer, in principle only a single pair of measurements for a single enantiomer with left- and right-handed CPL is necessary for its determination at any given energy using Eq. 2. The normalized intensities $I^p(\theta)$ are obtained from the experimental photoelectron intensities at a specified electron energy and detection angle θ , but require correction accounting for possible variation in photon flux and other sources of medium term experimental drift. Despite our best efforts to ensure that the fluxes of left- and right-handed CPL were equal — monitored via a photodiode — small persistent differences in light intensity of 1–3% remained and so data normalization was essential. In gas-phase PECD studies, 4π imaging spectrometers enable collection of the total ionization yield, and thus enable direct normalization.¹² In the present experimental arrangement the total ionization yield cannot be monitored and an alternative intensity-correction procedure utilizing the baseline signal was adopted. It is assumed that the background of scattered electrons is achiral and essentially independent of light polarization state. We therefore scaled all left- and right-handed CPL data (hereafter denoted as + and – spectra) to ensure equal intensity of the spectra at the low- and high-KE edges, where only an achiral background is present.

It is also vital that the baseline is accurately modeled such that the background beneath the peaks of interest can be reliably removed from the intensities I used to determine b_1^{+1} . It can be seen from Eq. 2 that while any residual background present in the suitably scaled I^+ and I^- will self-cancel in the numerator, this does not apply to the denominator, $[I^+ + I^-]$, whose magnitude would hence be overestimated, and lead to an erroneous underestimation of the derived $|b_1^{+1}|$ (see Fig. 3). This challenge is exacerbated for experiments with dilute chiral

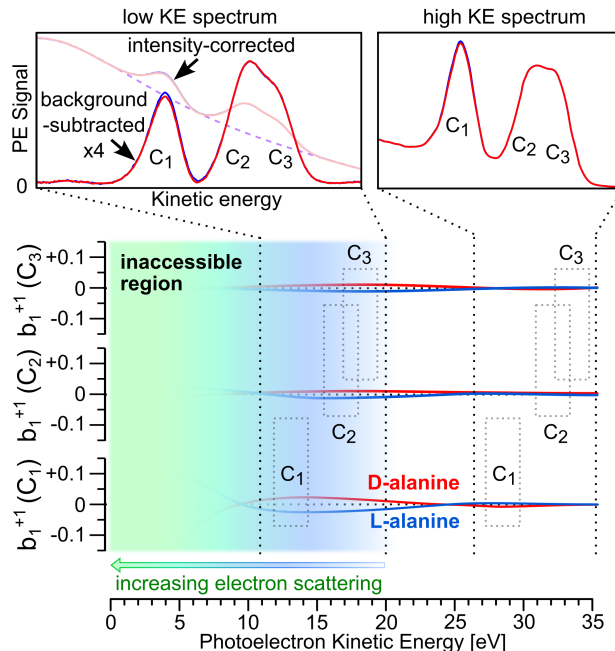


Figure 2: Top: Illustrative aqueous-phase (pH 13) alanine C 1s photoelectron spectra corresponding to right- and left-handed circularly polarized light (red and blue lines, respectively). The high-energy spectra (right) exhibit low background signal, but vanishing photoelectron circular dichroism (PECD). The low-energy spectra sit atop a large background signal, but reveal significant PECD following subtraction of background signal (purple lines). Bottom: Hypothetical b_1^{+1} parameters for each of alanine's carbon groups as a function of peak kinetic energy. The blue shaded zone represents the onset of significant kinetic-energy dependent elastic or quasi-elastic electron scattering. Within the green region, scattering of primary photoelectrons is sufficient to make resolution of the photoelectron features unfeasible. Values of b_1^{+1} are currently inaccessible for this system within this kinetic-energy range. Dashed gray boxes represent approximate peak positions for the spectra shown above. The carbon atoms C₁, C₂, and C₃ are identified in Fig. 1.

molecules where the signal-to-background ratio is much reduced (see Fig. 2, top). Details regarding the background-subtraction method employed may be found in the supporting information.

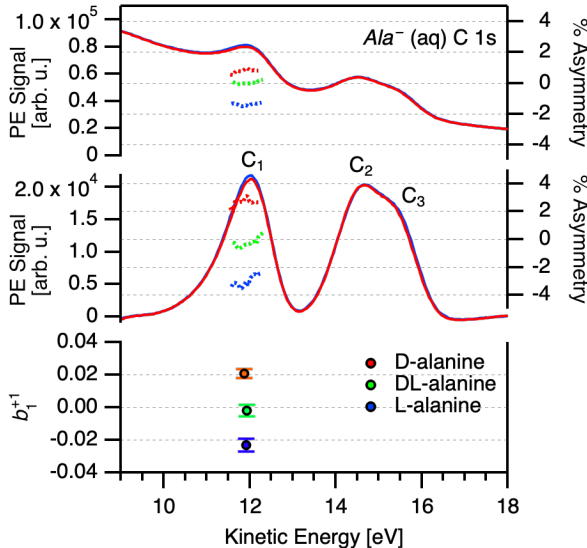


Figure 3: Top: Representative intensity-scaled C 1s photoelectron spectra of 1 M L-alanine aqueous solution (pH 13) measured at $h\nu = 305$ eV for left- and right-handed circularly polarized light (blue and red curves, respectively), along with the calculated percent difference between the spectra for C₁ group to background subtraction (right axis). Middle: Background-subtracted data, along with calculated percent difference between the spectra for C₁ (right axis). Bottom: Values of $b_1^{\pm 1}$ obtained through the same process for D-, L-, and racemic DL-alanine (red, blue, and green points, respectively). The error bars of these points represent the standard deviation of the percent-difference data shown in the middle panel. The spectra shown here are averages of ten acquisitions, as typical for the data discussed in this study.

At the near magic-angle geometry of $\theta = 50^\circ$ (in the backward direction) adopted for these experiments, the polynomial $P_2(\cos\theta) \neq 0$ and some residual influence of the $b_2^{\pm 1}$ parameter is unavoidably included in the measurement (see Eq. 2). However, there are currently no published values of $b_2^{\pm 1}$ for core-level photoionization of alanine. To obtain an estimate of the significance of the remnant $b_2^{\pm 1}$ contribution, we calculated the value of b_2^0 (β) for low-energy (KE = 0 to 25 eV) photoelectrons generated upon C 1s photoionization of gas-phase Ala^0 (details may be found in the supporting information, see Fig. S3). We found that for

photoionization of C_1 , the absolute value of β is less than 0.8 within this entire KE range, decreasing to less than 0.5 for photoelectrons with $KE < 15$ eV. Although aqueous-phase alanine will undoubtedly yield different values of β due to differences in conformation and the charge state of its functional groups, this calculation nevertheless provides a rough estimate. As a comparison, the measured value of β for O 1s photoionization of gas-phase water at 25 eV KE is approximately 1.6, whereas for liquid water at the same energy it is 0.6.³⁴ For both environments, β trends strongly toward 0 for lower photoelectron kinetic energies. This decrease in β as measured from liquid versus gaseous water was attributed primarily to highly efficient elastic or quasi-elastic scattering of photoelectrons by water molecules in the liquid. As water remains by far the likeliest scatterer of photoelectrons for the 1 M aqueous solutions of alanine studied in this work, it seems reasonable to expect a similar degree of PAD isotropization for β as measured in C 1s photoionization of these solutions. Conservatively assuming a β value of 0.5 as an upper limit for aqueous-phase alanine and using Eq. 2 while recalling that $b_2^{\pm 1} = -\beta/2$ and simply averaging over the acceptance angle of the analyzer ($\approx \pm 15^\circ$),²⁹ the effect would be to scale our measured values of $b_1^{\pm 1}$ by a factor of 0.97. Such a change does not alter the results of this study, and we do not consider it further in subsequent discussion.

For a given aqueous alanine solution (enantiomer, pH), we conducted C 1s LJ-PES measurements as a function of photon energy in the range of 302–310 eV, resulting in C_1 peaks in the KE range of 9–17 eV. For each photon energy, we measured 6–10 PE spectra before changing the polarization of the light, resulting in a measurement time of roughly 30–60 minutes per sample. We compared repeats using the same handedness of CPL for a given photon energy over time to ensure that our experimental conditions were reproducible during the measurement period.

In practice, and particularly due to the pioneering nature of this study, it is advantageous to determine $b_1^{\pm 1}$ for both enantiomers in order to detect any influence of instrumental and experimental asymmetry. Confirming the anticipated enantiomeric mirroring of the $b_1^{\pm 1}$ pa-

parameter assures the molecular origin of the observed asymmetry. Wherever possible, we also made the same observations for solutions of racemic DL-alanine, for which no asymmetry is expected. Due to the time-intensive nature of the experiments, which spanned multiple months of synchrotron measurements across four years, it was necessary to find a balance between the photoelectron KE range and enantiomer and protonation state of alanine investigated. This balance is reflected in the greater number of experimental data points measured for low-KE photoelectrons and for Ala^- (see for reference Figs. S4, S8, and S12).

Results and discussion

Following the process outlined in the supporting information and using Eq. 2, we determined a single value of b_1^{+1} per carbon center for each pair of + and - measurements for a given enantiomer, solution pH, and photon energy (Fig. 3). The data were then averaged within 250 meV KE windows for visualization. The complete datasets without averaging are presented in the supporting information (Figs. S5, S9, S13). The analysis was carried out blind with respect to the enantiomer, such that we analyzed all the data without knowing whether any given pair of measurements corresponded to a solution of L-, D-, or DL-alanine. An overview of the b_1^{+1} parameters obtained for C_1 at different pH values is presented in Fig. 4. Beginning with the pH 1 data, corresponding to Ala^+ , weak enantiomer-dependent asymmetry in b_1^{+1} may be seen for photoelectrons with KE 9 eV. At this energy, L-alanine exhibit a negative value of b_1^{+1} , while D-alanine yields a somewhat positive value. These values appear to rapidly trend toward zero at higher kinetic energies, and no significant PECD effect is found above 10 eV. For Ala^{zw} at pH 7, the situation is different. Here, b_1^{+1} is close to zero in the KE range of 9–11 eV, but appears to increase in magnitude briefly around 12–13 eV. From 14–16 eV, the data is noisy and does not indicate clear PECD. At 17 eV, b_1^{+1} increases once more. The sign of b_1^{+1} is the same for the corresponding enantiomer at pH 1. The clearest PECD can be seen for the case of Ala^- . For this protonation state, b_1^{+1} as measured

for C_1 is clearly non-zero for the entire KE range measured, even up to 17 eV. The sign of b_1^{+1} remains constant throughout the entire range, and is consistent with that observed for Ala^{zw} and Ala^+ .

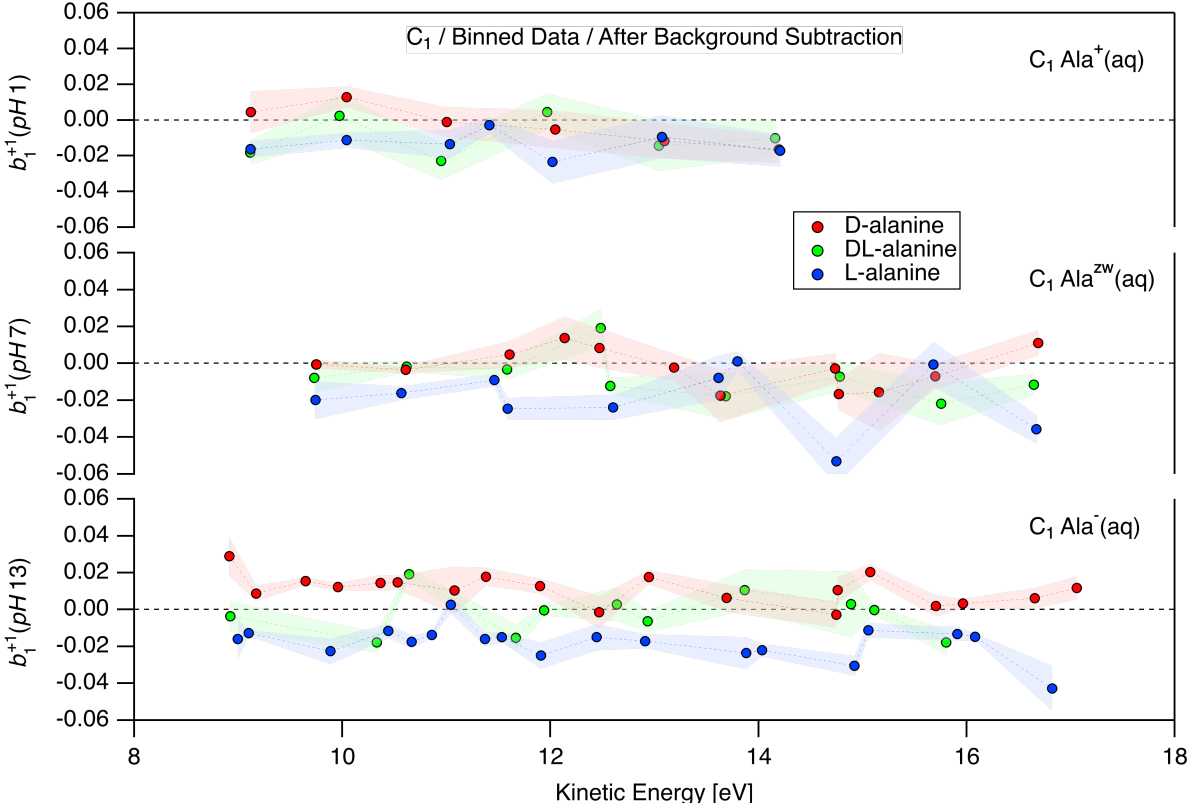


Figure 4: Values of the b_1^{+1} photoionization parameter obtained for C 1s measurements of aqueous solutions of D-, L-, and DL-alanine (red, blue, and green points, respectively) at pH 1, 7, and 13 (top, middle, and bottom; corresponding to the cationic, zwitterionic, and anionic form of the molecule, respectively). All b_1^{+1} values shown correspond to photoionization of the C_1 carboxylic group. The data displayed is the result of binning the results of individual measurement sets using a kinetic-energy window of 250 meV. The shaded error bars represent the combined error of the binned data points. A description of the error propagation may be found in the supporting information.

We were unable to conclusively identify signatures of PECD for the C_2 and C_3 atoms, with the possible exception of Ala^{zw} in the KE range of 15–19 eV (Figs. S8 and S9). However, due to the limited quantity of data in this KE range for Ala^{zw} and the overlapping nature of these peaks, we do not consider the C_2 and C_3 data to convincingly demonstrate PECD. As mentioned above, we dedicated the most time to collecting data points for Ala^- , which

appeared from the onset to yield the most clear PECD. As such, we are the most confident in our results for Ala^- . Although it may seem surprising that C_1 , C_2 , and C_3 should exhibit such large differences in PECD magnitude, significant site-dependent PECD has previously been reported in C 1s studies of carvone and fenchone,^{14,49} thereby highlighting the sensitivity of PECD to the atomic site probed. The datasets corresponding to Fig.4 for C_2 and C_3 are available in the supporting information (see Figs. S8 and S12).

Taken altogether, the data reveal a significant PECD effect for aqueous-phase alanine in photoionization of the C_1 carbon group, for all three of alanine’s protonation states. The sign of b_1^{+1} is consistent between Ala^+ , Ala^{zw} , and Ala^- , but differences in magnitude are apparent, with the most prominent effects measured for Ala^- . In contrast to most other PECD studies, we do not note a clear KE dependence for b_1^{+1} in our data. This is likely due to the compensation of increasing PECD by concomitantly increasing elastic scattering at low KEs (as illustrated in Fig. 2 within the blue and green regions). The extent to which the measured b_1^{+1} values will be reduced by scattering will depend on the specific KE-dependent elastic-scattering cross section. As such, substantial electron scattering may result in changes not only to the magnitude of the measured b_1^{+1} values, but also their apparent KE dependency. This result suggests that, for the current case of alanine in water, there may be limited experimental benefit (in terms of magnitude of measured b_1^{+1}) in focusing on very-low KE photoelectrons. As these low-KE spectra are the most difficult to analyze due to the necessity for significant background subtraction, follow-up studies may benefit from investigation of higher-energy (KE = 15–25 eV) photoelectrons. We can estimate the average degree of b_1^{+1} attenuation in our present measurements through comparison with previous work. As mentioned above, the angular asymmetry of the O 1s PAD is reduced by 60% for liquid compared to gaseous water at KE = 25 eV.³⁴ Similarly, in our previous core-level PECD study of liquid fenchone,³⁰ we reported a factor of 5 decrease for b_1^{+1} compared to that measured for gas-phase fenchone within the KE range of 9–13 eV.¹⁴ This seems to be a general trend upon condensation of chiral molecules; the magnitude of PECD measured for free serine

in the gas phase was also found to decrease upon condensation of serine into nanoparticles, although in this case condensation was also accompanied by changes of molecular charge state and conformer population, both of which influence PECD in a non-trivial manner.¹⁸ A more detailed understanding of elastic scattering of low-energy photoelectrons in aqueous solutions of alanine will be required to more accurately characterize the degree of isotropization in the present study. However, based on the work mentioned above, we estimate that our present results for b_1^{+1} may be attenuated by a factor of 3–5. For the C₁ data shown in Fig. 4, this means that our measured values of $b_1^{+1} \approx 0.02$ likely correspond to initial b_1^{+1} values of approximately 0.06–0.1 prior to deleterious photoelectron scattering. The above arguments equally hold for the C₂ and C₃ carbons and would serve to make what may have been initially low values b_1^{+1} for those atoms undetectable with the current experimental sensitivity.

Although no other core-level PECD studies of alanine have been published, we may compare our results with the existing theoretical and experimental investigations of valence-band PECD of alanine. These studies have revealed only modest PECD, with $b_1^{+1} \approx 0.02$, corresponding to a PECD effect of 4%.^{17,50} This value is roughly 10 times larger than the comparable ECD magnitude (g factor) for alanine in the gas phase,⁵¹ but significantly lower than the asymmetry reported for valence-band photoemission from rigid molecules such as terpenes (b_1^{+1} up to ≈ 0.1).⁵² The relatively weak PECD reported for alanine is similar to that observed for other flexible molecules in the gas phase, including alaninol,⁵³ indanol,^{22,37,54} endoborneol,⁵⁵ and proline,¹⁹ and may have to do with conformational averaging. Reflecting this conformational sensitivity, most PECD studies in the literature focus on relatively rigid molecules, including bicyclic terpenes and terpenoids,^{4,11–13,15,30,52,56,57} or other heterocyclic oxirane derivatives.^{8,10,58–62}

If core-level photoionization of alanine’s C₂ and C₃ atoms in the gas phase were to result in similar values as measured for valence-band photoionization of alanine ($b_1^{+1} \approx 0.02$), they would likely manifest in our experiments as $b_1^{+1} \approx 0.004$ – 0.007 (based on our scattering estimate above). As can be seen in Fig. 4, the conclusive detection of such low values is

currently not feasible. Considering the general trend of flexible molecules exhibiting weaker PECD, it appears reasonable that we currently lack the sensitivity to PECD from all of alanine’s carbon groups. Somewhat more surprising is that, despite elastic scattering, our measured values of b_1^1 for core-level photoionization of C₁ in aqueous Ala^- are comparable to those reported for valence-band photoionization of gas-phase Ala^0 .

The specific details, signs, and magnitudes of PECD arise as results of extensive interference between multiple continuum partial electron waves upon photoionization, and thus defy intuitive prediction.⁴⁷ Nevertheless, it is clear that the local scattering environment must necessarily influence the continuum wave function of each partial electron wave. The significant role of final-state scattering in core-level PECD was first experimentally demonstrated in C 1s photoionization of gaseous carvone and fenchone, for which strong PECD was observed despite the spherical symmetry of the initial states.^{14,49} As our present study constitutes the only report of PECD of aqueous-phase systems at this time, it is useful to briefly discuss how some of the most prominent differences between aqueous-phase and gas-phase molecules may manifest in PECD measurements. Theoretical approaches to determining PECD are currently limited to small gas-phase molecules, and we hope that the following discussion will stimulate the development of new methods capable of modeling PECD for aqueous-phase systems, which we anticipate will prove invaluable for the the application of liquid-jet PECD as a practical analytical technique. We suggest that a model of PECD for zwitterionic alanine microsolvated by 5 explicit water molecules — the minimum required to stabilize the charged forms of alanine in solution⁶³ — would constitute a valuable step in this direction.

In general, the changes in local electron density following protonation / deprotonation of the NH_2/NH_3^+ and $COOH/COO^-$ groups will be reflected in the electronic scattering potential. Previously published work comparing PECD in anionic and neutral gas-phase species has revealed both qualitative and quantitative differences in PECD depending on charge state,³⁵⁻³⁷ and time-resolved experiments have identified significant differences for

core-level PECD of fenchone in the electronic ground versus excited 3s Rydberg state,⁶⁴ thereby convincingly demonstrating PECD's sensitivity to nearly any change in electronic structure. Thus, the differences in charge state for alanine in solution might alone be sufficient to explain the pH-dependent PECD that we observe. However, this conclusion would ignore explicit solvent-solute interactions, which we expect to play a major role in modulating PECD for aqueous-phase chiral molecules.

The most energetically favorable conformations of alanine in the gas phase are stabilized by intramolecular hydrogen-bond formation between the NH_2 and COOH groups.⁶⁵⁻⁶⁷ These intramolecular hydrogen bonds will likely be disrupted in solution, being replaced by intermolecular alanine-solvent interactions. The loss of intramolecular hydrogen bonds may result in subtle changes to PECD, as intramolecular hydrogen-bond orbital polarization has been shown to play a small yet significant role in determining chiral PAD asymmetry.⁶⁸ The relevance of intermolecular interactions for PECD has been revealed through studies of homochiral clusters of small, weakly interacting molecules, for which profound changes in PECD were observed between isolated monomers, dimers, and larger "n-mers".^{16,69} In the present context, the formation of new intermolecular hydrogen bonds between water and alanine will almost certainly substantially influence the measured PECD. We also note that a molecule's lowest-energy conformers well may differ between the gas and solution phases,⁴⁶ and that such differences would be associated with changes in the nuclear scattering potential and the consequent PECD signal.

Although only little work focused on the solvation environment of alanine in solution across its different protonation states exists, we will attempt to sketch a preliminary model based on the current state of the literature. In the case of Ala^{zw} , water molecules readily hydrogen bond to the charged COO^- and NH_3^+ groups, forming a bridge between them and thus stabilizing the doubly ionized form of the molecule.^{63,70-72} At this pH, water molecules slightly prefer bonding to COO^- , forming on average six bonds with that group compared to three with NH_3^+ .⁷³ This preference of water to form hydrogen bonds with the COO^- group is

consistent for Ala^- and is also similar to what has been previously reported for zwitterionic glycine in water.⁷⁴ Under acidic conditions, the trend seems to invert, with four waters preferentially coordinating to the NH_3^+ group and only two to the COOH group.⁷³ Simulations of alanine in the presence of larger numbers of explicit water molecules have demonstrated that alanine–water complexes are dynamic, with alanine’s different functional groups capable of rotating, and with hydrogen-bonded water molecules within the first solvation shell constantly exchanging with those from the second.⁷⁰ However, these processes occur on the ps scale, and while they may be significant for time-resolved PECD studies, alanine’s solvation shell appears relatively structured and rigid averaged over the time scale of minutes, with the charged functional groups hydrogen-bonded to water molecules more than 95% of the time.^{70,71} Even alanine’s methyl group, which does not form strong hydrogen bonds with water, seems to be involved in the formation of a structured screening water network⁷⁵ These studies identify large differences in the degree of hydrogen bonding between water molecules and alanine’s different functional groups depending on pH, which may partially explain the site- and protonation-state-dependent PECD that we have measured.

PECD has recently been reported for gas-phase photoionization of an achiral chromophore weakly bound to a chiral molecule, indicating that PECD exhibits long-range (on the 5 Å scale) sensitivity to chirality.⁷⁶ As such, PECD of aqueous-phase chiral molecules is almost certain to be sensitive to induced solvent chirality within the first solvation shell. The extent to which induced chirality may arise in a solvation shell appears to depend strongly on solvent polarizability and the van der Waals volume of the solvent molecule.^{28,77,78} Chiral sum frequency generation (SFG) spectroscopy experiments probing induced chirality in the solvation shell around small proteins near the liquid-vapor interface have revealed that the most significant chiral signal from the solvent originates within the first solvation shell, with the second and third solvation shells being nearly achiral.⁷⁹ These conclusions are in agreement with results from molecular dynamics simulations⁷⁸ and suggest an analogy of molecules in the first solvation behaving cooperatively as an achiral glove (for example, a

non-handed nitrile glove), adopting a preferential handedness only upon being worn (or upon solvating a chiral solute). The consequences of induced chirality for chiral spectroscopy can be significant, as in the case of methyloxirane in benzene, for which the ECD signal appears to be dominated by the solvation-shell structure rather than by the intrinsically chiral solute itself.⁸⁰ Vibrational circular dichroism (VCD), probing the difference in absorption of left- and right-handed CPL in the infrared and near-infrared region, has also proven capable of resolving signatures of chirality transfer between solute and solvent via hydrogen bonding.^{81–84} Although the chirality of alanine’s aqueous solvation shell has not yet been studied directly, all criteria seem to be met for the formation of a chiral solvation shell. We note that the ECD response of *Ala^{zw}* differs substantially in the solid vs. in the liquid phase⁸⁵ and in general the ECD spectra of aqueous-phase alanine is dependent on solution pH,³ but it is presently unclear whether these trends are related to solvent effects, or simply due to differences in solute conformation or protonation state. We suggest that molecular dynamics studies investigating the chirality of aqueous-phase alanine’s solvation shell as a function of protonation state, combined with new approaches to calculating PECD for larger systems, will be of direct relevance for interpreting our present experimental results. The chirality of a solvation shell will likely manifest differently for different chiral spectroscopic techniques. ECD and VCD appear capable of revealing general chiral effects in the solvation shell, and chiral SFG is well suited for studying molecules at the liquid-vapor interface. Due to its site specificity, core-level PECD may enable much more localized probing of chiral solvation effects, both for bulk-soluble and surface-active molecules. This study constitutes an important first step in this direction.

Importantly, we note that although PECD of aqueous-phase chiral molecules currently requires time-intensive measurement, new experimental approaches that enable simultaneous detection of photoelectrons in both the forward and backward directions with enhanced detection efficiency would dramatically expand the general applicability of this method. In particular, we highlight liquid-compatible velocity map imaging as a technique of consider-

able interest for the further development of LJ-PECD.⁸⁶

Conclusions

We have measured core-level photoelectron circular dichroism (PECD) for aqueous-phase alanine, the smallest chiral amino acid, for each of its three charge states (cationic, zwitterionic, and anionic). We detected significant PECD for photoionization of alanine’s carboxylic acid functional group, which exhibited a clear magnitude dependence across pH conditions, but did not exhibit a strong kinetic-energy dependence. We attribute the latter observation to significant kinetic-energy dependent elastic scattering of low-energy primary photoelectrons. We did not measure significant PECD in photoionization of alanine’s chiral center or methyl group, suggesting that the effects for those groups are weak and below our currently modest experimental sensitivity. For photoionization of the carboxylic acid, PECD is the most pronounced under basic solution conditions, where alanine adopts the anionic form, decreases for the zwitterionic form, and is very weak for the cationic form. The differences observed across protonation states may be due to a number of factors, including changes in molecular charge state, functional-group dependent solute-solvent interactions, and first solvation-shell structure. Advances in computational approaches for modeling PECD in multiple-molecule systems will be necessary to identify the relative weights of these effects, and higher collection efficiency detectors capable of simultaneous measurement in the forward and backward direction will dramatically simplify its application in the future. Our demonstration of aqueous-phase PECD marks a significant advance in the field of liquid-jet photoelectron spectroscopy. Given its chemical-state and site specificity and enantiomeric sensitivity, liquid-phase PECD is likely to become a remarkably useful analytical method for studying chiral molecules under biologically relevant aqueous conditions.

Experimental

We carried out all aqueous-phase PECD experiments using our custom LJ-PES apparatus — Electronic Structure from Aqueous Solutions and Interfaces (EASI) — developed specifically for this purpose.²⁹ We introduced alanine aqueous solutions into the experimental chamber using a custom quartz capillary, with an inner diameter on the order of 20–30 μm . Solutions were driven by a high-performance liquid chromatography pump (Shimadzu LC-20AD) at a flow rate of 0.8–1.5 mL/minute, resulting in solution velocities of 20–80 m/s. The solutions were prepared by diluting alanine in water, adjusting solution pH where necessary with concentrated HCl or solid NaOH, and finally diluting the solution to reach a final concentration of 1 M alanine. The solutions were injected horizontally and frozen out after the interaction region via contact with a liquid-nitrogen-cooled cold trap. All PES experiments were performed at the P04 soft x-ray beamline of the PETRA III storage ring at DESY in Hamburg, Germany. Critically, the P04 beamline is equipped with an APPLE-II undulator, enabling experiments with circularly polarized light within the experimentally relevant photon-energy range of 290–320 eV.⁸⁷ Although not available during our early measurements, recent advancements at the P04 beamline now enable the estimation of the degree of circular polarization for a given set of undulator conditions. Retroactive estimates revealed an expected circular polarization of >99% for all experimental conditions employed in this study. D-, L-, and DL-alanine (>98% purity) were purchased from Sigma-Aldrich and Carl Roth and used as received. Enantiomeric purity was confirmed via intermittent testing using ECD (see Figure S2). For additional experimental details regarding our instrumentation or LJ-PES more generally, we direct interested readers to our recent technical publication.²⁹ All data reduction was performed using the Igor Pro analysis software (Wavemetrics, version 9).

Acknowledgement

We acknowledge DESY (Hamburg, Germany), a member of the Helmholtz Association (HGF), for the provision of experimental facilities. Parts of this research were carried out at PETRA III at the P04 soft x-ray beamline. Beamtime was allocated for proposals II-20180012, I-20200682, II-20210015, I-20211126, and I-20230378. We thank the P04 beamline staff, in particular Dr. Moritz Hoesch and Jörn Seltmann, for their long-standing support for this project. We also thank the European Molecular Biology Laboratory for access to the circular dichroism spectrophotometer. We thank Prof. Petr Slavíček, Prof. Philipp Demekhin, former group members Dr. Anne Stephansen, Dr. Claudia Kolbeck, Dr. Marvin Pohl, Dr. Karen Mudryk, and Dr. Tillmann Buttersack, as well as current group members Harmanjot Kaur, Qi Zhou, Dr. Lukáš Tomaník, Dr. Nicolas Velasquez, Henrik Haak, and Sebastian Kray for valuable discussion and assistance with the transportation and preparation of our setup (EASI) for measurements at PETRA III.

D.S., U.H., M.P., B.C., and B.W. acknowledge funding from the European Research Council (ERC) under the European Union’s Horizon 2020 research and innovation program under Grant Agreement No. GAP 883759–AQUACHIRAL. F.T. acknowledges funding by the Deutsche Forschungsgemeinschaft (DFG, German Research Foundation) - Project 509471550, Emmy Noether Programme. F.T. and B.W. acknowledges support by the MaxWater initiative of the Max-Planck-Gesellschaft. B.W. acknowledges support by the Deutsche Forschungsgemeinschaft (Wi 1327/5-1). S.T. acknowledges support from ISHIZUE 2024 of Kyoto University.

Supporting Information Available

The supporting information contains electronic circular dichroism measurements of aqueous solutions of alanine, calculations of the photoionization parameter b_2^0 in the kinetic-energy range of 0–25 eV, a summary of all values of b_1^{+1} measured for alanine’s different carbon

groups, including values calculated before background subtraction and kinetic-energy averaging was performed, and a description of the means determining the error of the b_1^{+1} values, as shown in Figures 3 and 4.

The data of relevance to this study may be accessed at the following DOI: 10.5281/zenodo.13902253.

References

- (1) Quack, M.; Stohner, J.; Willeke, M. High-resolution spectroscopic studies and theory of parity violation in chiral molecules. *Annu. Rev. Phys. Chem.* **2008**, *59*, 741–769.
- (2) Berova, N.; Bari, L. D.; Pescitelli, G. Application of electronic circular dichroism in configurational and conformational analysis of organic compounds. *Chemical Society Reviews* **2007**, *36*, 914.
- (3) Nishino, H.; Kosaka, A.; Hembury, G. A.; Matsushima, K.; Inoue, Y. The pH dependence of the anisotropy factors of essential amino acids. *J. Chem. Soc., Perkin Trans. 2* **2002**, 582–590.
- (4) Böwering, N.; Lischke, T.; Schmidtke, B.; Müller, N.; Khalil, T.; Heinzmann, U. Asymmetry in photoelectron emission from chiral molecules induced by circularly polarized light. *Phys. Rev. Lett.* **2001**, *86*, 1187.
- (5) Ritchie, B. Theory of the angular distribution of photoelectrons ejected from optically active molecules and molecular negative ions. *Phys. Rev. A* **1976**, *13*, 1411.
- (6) Ritchie, B. Theory of angular distribution for ejection of photoelectrons from optically active molecules and molecular negative ions. II. *Phys. Rev. A* **1976**, *14*, 359.
- (7) Nahon, L.; Garcia, G. A.; Powis, I. Valence shell one-photon photoelectron circular dichroism in chiral systems. *J Electron Spectrosc.* **2015**, *204*, 322–334.

- (8) Tia, M. et al. Observation of Enhanced Chiral Asymmetries in the Inner-Shell Photoionization of Uniaxially Oriented Methyloxirane Enantiomers. *J. Phys. Chem. Lett.* **2017**, *8*, 2780–2786.
- (9) Fehre, K. et al. Fourfold Differential Photoelectron Circular Dichroism. *Phys. Rev. Lett.* **2021**, *127*, 103201.
- (10) Nalin, G. et al. Molecular-frame differential photoelectron circular dichroism of O 1s photoelectrons of trifluoromethyloxirane. *Phys. Rev. Res.* **2023**, *5*, 013021.
- (11) Hergenbahn, U.; Rennie, E. E.; Kugeler, O.; Marburger, S.; Lischke, T.; Powis, I.; Garcia, G. Photoelectron circular dichroism in core level ionization of randomly oriented pure enantiomers of the chiral molecule camphor. *J. Chem. Phys.* **2004**, *120*, 4553–4556.
- (12) Nahon, L.; Garcia, G. A.; Harding, C. J.; Mikajlo, E.; Powis, I. Determination of chiral asymmetries in the valence photoionization of camphor enantiomers by photoelectron imaging using tunable circularly polarized light. *J. Chem. Phys.* **2006**, *125*, 114309.
- (13) Powis, I.; Harding, C. J.; Garcia, G. A.; Nahon, L. A Valence Photoelectron Imaging Investigation of Chiral Asymmetry in the Photoionization of Fenchone and Camphor. *ChemPhysChem* **2008**, *9*, 475–483.
- (14) Ulrich, V.; Barth, S.; Joshi, S.; Hergenbahn, U.; Mikajlo, E.; Harding, C. J.; Powis, I. Giant Chiral Asymmetry in the C 1s Core Level Photoemission from Randomly Oriented Fenchone Enantiomers. *J. Phys. Chem. A* **2008**, *112*, 3544–3549.
- (15) Nahon, L.; Garcia, G. A.; Soldi-Lose, H.; Daly, S.; Powis, I. Effects of dimerization on the photoelectron angular distribution parameters from chiral camphor enantiomers obtained with circularly polarized vacuum-ultraviolet radiation. *Phys. Rev. A* **2010**, *82*, 032514.

- (16) Powis, I.; Daly, S.; Tia, M.; Cunha de Miranda, B.; Garcia, G. A.; Nahon, L. A Photoionization Investigation of Small, Homochiral Clusters of Glycidol using Circularly Polarized Radiation and Velocity Map Electron-Ion Coincidence Imaging. *Phys. Chem. Chem. Phys.* **2014**, *16*, 467–476.
- (17) Tia, M.; Cunha De Miranda, B.; Daly, S.; Gaie-Levrel, F.; Garcia, G. A.; Powis, I.; Nahon, L. Chiral asymmetry in the photoionization of gas-phase amino-acid alanine at lyman-alpha radiation wavelength. *J. Phys. Chem. Lett.* **2013**, *4*, 2698–2704.
- (18) Hartweg, S.; Garcia, G. A.; Božanić, D. K.; Nahon, L. Condensation Effects on Electron Chiral Asymmetries in the Photoionization of Serine: From Free Molecules to Nanoparticles. *J. Phys. Chem. Lett.* **2021**, *12*, 2385–2393.
- (19) Hadidi, R.; Božanić, D. K.; Ganjtabar, H.; Garcia, G. A.; Powis, I.; Nahon, L. Conformer-dependent vacuum ultraviolet photodynamics and chiral asymmetries in pure enantiomers of gas phase proline. *Commun. Chem.* **2021**, *4*, 72.
- (20) Darquié, B.; Saleh, N.; Tokunaga, S. K.; Srebro-Hooper, M.; Ponzi, A.; Autschbach, J.; Decleva, P.; Garcia, G. A.; Crassous, J.; Nahon, L. Valence-shell photoelectron circular dichroism of ruthenium(iii)-tris-(acetylacetonato) gas-phase enantiomers. *Phys. Chem. Chem. Phys.* **2021**, *23*, 24140–24153.
- (21) Turchini, S. Conformational effects in photoelectron circular dichroism. *Journal of Physics: Condensed Matter* **2017**, *29*, 503001.
- (22) Rouquet, E.; Dupont, J.; Lepere, V.; Garcia, G. A.; Nahon, L.; Zehnacker, A. Conformer-Selective Photoelectron Circular Dichroism. *Angew. Chem. Int. Ed.* **2024**, *63*, e202401423.
- (23) Beaulieu, S.; Ferré, A.; Généaux, R.; Canonge, R.; Descamps, D.; Fabre, B.; Fedorov, N.; Légaré, F.; Petit, S.; Ruchon, T.; Blanchet, V.; Mairesse, Y.; Pons, B. Uni-

- versality of photoelectron circular dichroism in the photoionization of chiral molecules. *New Journal of Physics* **2016**, *18*, 102002.
- (24) Lehmann, C. S.; Ram, N. B.; Powis, I.; Janssen, M. H. M. Imaging photoelectron circular dichroism of chiral molecules by femtosecond multiphoton coincidence detection. *J. Chem. Phys.* **2013**, *139*, 234307.
- (25) Lux, C.; Wollenhaupt, M.; Bolze, T.; Liang, Q.; Köhler, J.; Sarpe, C.; Baumert, T. Circular Dichroism in the Photoelectron Angular Distributions of Camphor and Fenchone from Multiphoton Ionization with Femtosecond Laser Pulses. *Angew. Chem. Int. Ed* **2012**, *51*, 5001–5005.
- (26) Levy, Y.; Onuchic, J. N. Water Mediation In Protein Folding and Molecular Recognition. *Annu. Rev. Biophys.* **2006**, *35*, 389–415.
- (27) Mennucci, B.; Cappelli, C.; Cammi, R.; Tomasi, J. Modeling solvent effects on chiroptical properties. *Chirality* **2011**, *23*, 717–729.
- (28) Fidler, J.; Rodger, P. M.; Rodger, A. Circular dichroism as a probe of chiral solvent structure around chiral molecules. *J. Chem. Soc., Perkin Trans. 2* **1993**, 235–241.
- (29) Malerz, S.; Haak, H.; Trinter, F.; Stephansen, A. B.; Kolbeck, C.; Pohl, M.; Hergen- hahn, U.; Meijer, G.; Winter, B. A setup for studies of photoelectron circular dichroism from chiral molecules in aqueous solution. *Rev. Sci. Instrum.* **2022**, *93*, 015101.
- (30) Pohl, M. N.; Malerz, S.; Trinter, F.; Lee, C.; Kolbeck, C.; Wilkinson, I.; Thürmer, S.; Neumark, D. M.; Nahon, L.; Powis, I.; Meijer, G.; Winter, B.; Hergen- hahn, U. Photo- electron circular dichroism in angle-resolved photoemission from liquid fenchone. *Phys. Chem. Chem. Phys.* **2022**, *24*, 8081–8092.
- (31) Winter, B.; Faubel, M. Photoemission from liquid aqueous solutions. *Chemical Reviews* **2006**, *106*, 1176–1211.

- (32) Seidel, R.; Winter, B.; Bradforth, S. E. Valence Electronic Structure of Aqueous Solutions: Insights from Photoelectron Spectroscopy. *Annu. Rev. Phys. Chem.* **2016**, *67*, 283–305.
- (33) Malerz, S. et al. Low-energy constraints on photoelectron spectra measured from liquid water and aqueous solutions. *Phys. Chem. Chem. Phys.* **2021**, *23*, 8246–8260.
- (34) Thürmer, S.; Seidel, R.; Faubel, M.; Eberhardt, W.; Hemminger, J. C.; Bradforth, S. E.; Winter, B. Photoelectron angular distributions from liquid water: Effects of electron scattering. *Phys. Rev. Lett.* **2013**, *111*, 173005.
- (35) Krüger, P.; Weitzel, K.-M. Photoelectron Circular Dichroism in the Photodetachment of Amino Acid Anions. *Angew. Chem. Int. Ed.* **2021**, *60*, 17861–17865.
- (36) Krüger, P.; Both, J. H.; Linne, U.; Chirot, F.; Weitzel, K.-M. Photoelectron Circular Dichroism of Electrosprayed Gramicidin Anions. *J. Phys. Chem. Lett.* **2022**, *13*, 6110–6116.
- (37) Triptow, J.; Fielicke, A.; Meijer, G.; Green, M. Imaging Photoelectron Circular Dichroism in the Detachment of Mass-Selected Chiral Anions. *Angew. Chem. Int. Ed.* **2023**, *62*, e202212020.
- (38) Thürmer, S.; Malerz, S.; Trinter, F.; Hergenbahn, U.; Lee, C.; Neumark, D. M.; Meijer, G.; Winter, B.; Wilkinson, I. Accurate vertical ionization energy and work function determinations of liquid water and aqueous solutions. *Chem. Sci.* **2021**, *12*, 10558–10582.
- (39) Credidio, B.; Pugini, M.; Malerz, S.; Trinter, F.; Hergenbahn, U.; Wilkinson, I.; Thürmer, S.; Winter, B. Quantitative electronic structure and work-function changes of liquid water induced by solute. *Phys. Chem. Chem. Phys.* **2022**, *24*, 1310–1325.

- (40) Pugini, M.; Credidio, B.; Walter, I.; Malerz, S.; Trinter, F.; Stemer, D.; Hergenahhn, U.; Meijer, G.; Wilkinson, I.; Winter, B.; Thürmer, S. How to measure work functions from aqueous solutions. *Chem. Sci.* **2023**, *14*, 9574–9588.
- (41) Kurahashi, N.; Karashima, S.; Tang, Y.; Horio, T.; Abulimiti, B.; Suzuki, Y.-I.; Ogi, Y.; Oura, M.; Suzuki, T. Photoelectron spectroscopy of aqueous solutions: Streaming potentials of NaX (X = Cl, Br, and I) solutions and electron binding energies of liquid water and X⁻. *J. Chem. Phys.* **2014**, *140*, 174506.
- (42) Pohl, M. N.; Muchová, E.; Seidel, R.; Ali, H.; Sršěň, S.; Wilkinson, I.; Winter, B.; Slavíček, P. Do water’s electrons care about electrolytes? *Chem. Sci.* **2019**, *10*, 848–865.
- (43) Winter, B.; Thürmer, S.; Wilkinson, I. Absolute Electronic Energetics and Quantitative Work Functions of Liquids from Photoelectron Spectroscopy. *Acc. Chem. Res.* **2023**, *56*, 77–85.
- (44) Clark, D. T.; Peeling, J.; Colling, L. An experimental and theoretical investigation of the core level spectra of a series of amino acids, dipeptides and polypeptides. *Biochim. Biophys. Acta* **1976**, *453*, 533–545.
- (45) Powis, I.; Rennie, E. E.; Hergenahhn, U.; Kugeler, O.; Bussy-Socrate, R. Investigation of the gas-phase amino acid alanine by synchrotron radiation photoelectron spectroscopy. *J. Phys. Chem. A* **2003**, *107*, 25–34.
- (46) Credidio, B.; Thürmer, S.; Stemer, D.; Pugini, M.; Trinter, F.; Vokrouhlicky, J.; Slavicek, P.; Winter, B. From Gas to Solution: The Changing Neutral Structure of Proline Upon Solvation. *J. Phys. Chem. A* **2024**, *Accepted for Publication*, DOI: 10.1021/acs.jpca.4c05628.
- (47) Powis, I. In *Advances in Chemical Physics*; Rice, S. A., Ed.; John Wiley & Sons, Inc.: Hoboken, NJ, USA, 2008; Vol. 138; pp 267–329.

- (48) Reid, K. L. Photoelectron angular distributions. *Annu. Rev. Phys. Chem.* **2003**, *54*, 397–424.
- (49) Harding, C. J.; Mikajlo, E. A.; Powis, I.; Barth, S.; Joshi, S.; Ulrich, V.; Hergenahm, U. Circular Dichroism in the Angle-Resolved C 1s Photoemission Spectroscopy of Gas-Phase Carvone Enantiomers. *J. Chem. Phys.* **2005**, *123*, 234310.
- (50) Tia, M.; Cunha De Miranda, B.; Daly, S.; Gaie-Levrel, F.; Garcia, G. A.; Nahon, L.; Powis, I. VUV photodynamics and chiral asymmetry in the photoionization of gas phase alanine enantiomers. *J. Phys. Chem. A* **2014**, *118*, 2765–2779.
- (51) Meinert, C.; Garcia, A. D.; Topin, J.; Jones, N. C.; Diekmann, M.; Berger, R.; Nahon, L.; Hoffmann, S. V.; Meierhenrich, U. J. Amino acid gas phase circular dichroism and implications for the origin of biomolecular asymmetry. *Nat. Commun.* **2022**, *13*, 1–7.
- (52) Nahon, L.; Nag, L.; Garcia, G. A.; Myrgorodska, I.; Meierhenrich, U.; Beaulieu, S.; Wanie, V.; Blanchet, V.; Géneaux, R.; Powis, I. Determination of accurate electron chiral asymmetries in fenchone and camphor in the VUV range: Sensitivity to isomerism and enantiomeric purity. *Phys. Chem. Chem. Phys.* **2016**, *18*, 12696–12706.
- (53) Turchini, S.; Catone, D.; Contini, G.; Zema, N.; Irrera, S.; Stener, M.; Di Tommaso, D.; Decleva, P.; Prospero, T. Conformational effects in photoelectron circular dichroism of alaninol. *ChemPhysChem* **2009**, *10*, 1839–1846.
- (54) Dupont, J.; Lepère, V.; Zehnacker, A.; Hartweg, S.; Garcia, G. A.; Nahon, L. Photoelectron Circular Dichroism as a Signature of Subtle Conformational Changes: The Case of Ring Inversion in 1-Indanol. *J. Phys. Chem. Lett.* **2022**, *13*, 2313–2320.
- (55) Garcia, G. A.; Soldi-Lose, H.; Nahon, L.; Powis, I. Photoelectron Circular Dichroism Spectroscopy in an Orbital Congested System: The Terpene Endoborneol. *J. Phys. Chem. A* **2010**, *114*, 847–853.

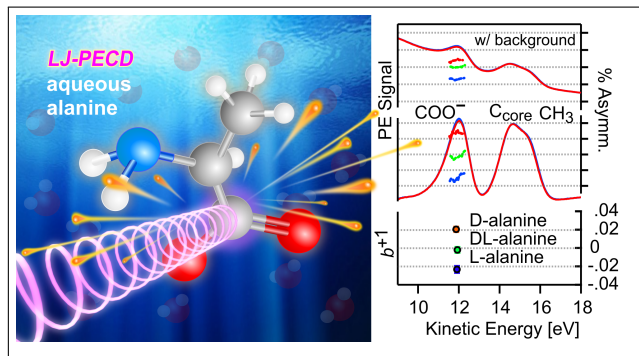
- (56) Lischke, T.; Böwering, N.; Schmidtke, B.; Müller, N.; Khalil, T.; Heinzmann, U. Circular dichroism in valence photoelectron spectroscopy of free unoriented chiral molecules: Camphor and bromocamphor. *Phys. Rev. A* **2004**, *70*, 022507.
- (57) Ganjitabar, H.; Hadidi, R.; Garcia, G. A.; Nahon, L.; Powis, I. Vibrationally-resolved photoelectron spectroscopy and photoelectron circular dichroism of bicyclic monoterpene enantiomers. *J Mol. Spectrosc.* **2018**, *353*, 11–19.
- (58) Stranges, S.; Alagia, M.; Decleva, P.; Stener, M.; Fronzoni, G.; Toffoli, D.; Speranza, M.; Catone, D.; Turchini, S.; Prospero, T.; Zema, N.; Contini, G.; Keheyan, Y. The valence electronic structure and conformational flexibility of epichlorohydrin. *Phys. Chem. Chem. Phys.* **2011**, *13*, 12517.
- (59) Garcia, G. A.; Dossmann, H.; Nahon, L.; Daly, S.; Powis, I. Photoelectron circular dichroism and spectroscopy of trifluoromethyl- and methyl-oxirane: a comparative study. *Phys. Chem. Chem. Phys.* **2014**, *16*, 16214–16224.
- (60) Ilchen, M. et al. Emitter-site-selective photoelectron circular dichroism of trifluoromethyloxirane. *Phys. Rev. A* **2017**, *95*, 053423.
- (61) Nalin, G. et al. Photoelectron circular dichroism of O 1s-photoelectrons of uniaxially oriented trifluoromethyloxirane: energy dependence and sensitivity to molecular configuration. *Phys. Chem. Chem. Phys.* **2021**, *23*, 17248–17258.
- (62) Fehre, K.; Trinter, F.; Novikovskiy, N. M.; Grundmann, S.; Tsitsonis, D.; Eckart, S.; Bauer, L.; Hilzinger, M.; Jahnke, T.; Dörner, R.; Demekhin, P. V.; Schöffler, M. S. Influence of the emission site on the photoelectron circular dichroism in trifluoromethyloxirane. *Phys. Chem. Chem. Phys.* **2022**, *24*, 13597–13604.
- (63) Mullin, J. M.; Gordon, M. S. Alanine: Then There Was Water. *J. Phys. Chem. B* **2009**, *113*, 8657–8669.

- (64) Facciala, D. et al. Time-Resolved Chiral X-Ray Photoelectron Spectroscopy with Transiently Enhanced Atomic Site Selectivity: A Free-Electron Laser Investigation of Electronically Excited Fenchone Enantiomers. *Phys. Rev. X* **2023**, *13*, 011044.
- (65) Császár, A. G. Conformers of Gaseous α -Alanine. *J. Phys. Chem.* **1996**, *100*, 3541–3551.
- (66) Blanco, S.; Lesarri, A.; López, J. C.; Alonso, J. L. The Gas-Phase Structure of Alanine. *J. Am. Chem. Soc.* **2004**, *126*, 11675–11683.
- (67) Balabin, R. M. The identification of the two missing conformers of gas-phase alanine: a jet-cooled Raman spectroscopy study. *Phys. Chem. Chem. Phys.* **2010**, *12*, 5980–5982.
- (68) Garcia, G. A.; Nahon, L.; Harding, C. J.; Powis, I. Chiral Signatures in Angle Resolved Valence Photoelectron Spectroscopy of Pure Glycidol Enantiomers. *Phys. Chem. Chem. Phys.* **2008**, *10*, 1628–1639.
- (69) Daly, S.; Powis, I.; Garcia, G.; Soldi-Lose, H.; Nahon, L. Photoionization of epichlorohydrin enantiomers and clusters studied with circularly polarized VUV radiation. *J. Chem. Phys.* **2011**, *134*, 064306.
- (70) Degtyarenko, I. M.; Jalkanen, K. J.; Gurtovenko, A. A.; Nieminen, R. M. Alanine in a Droplet of Water: A Density-Functional Molecular Dynamics Study. *J. Phys. Chem. B* **2007**, *111*, 4227–4234.
- (71) Degtyarenko, I.; Jalkanen, K. J.; Gurtovenko, A. A.; Nieminen, R. M. The Aqueous and Crystalline Forms of L-Alanine Zwitterion. *Journal of Computational and Theoretical Nanoscience* **2008**, *5*, 277–285.
- (72) Mullin, J. M.; Gordon, M. S. Water and Alanine: From Puddles(32) to Ponds(49). *J. Phys. Chem. B* **2009**, *113*, 14413–14420.

- (73) Ludwig, V.; da Costa Ludwig, Z. M.; Valverde, D.; Georg, H. C.; Canuto, S. Free energy gradient for understanding the stability and properties of neutral and charged L-alanine molecule in water. *J. Mol. Liq.* **2020**, *319*, 114109.
- (74) Sun, J.; Bousquet, D.; Forbert, H.; Marx, D. Glycine in aqueous solution: solvation shells, interfacial water, and vibrational spectroscopy from *ab initio* molecular dynamics. *J. Chem. Phys.* **2010**, *133*, 114508.
- (75) Panuszko, A.; Adamczak, B.; Czub, J.; Gojło, E.; Stangret, J. Hydration of amino acids: FTIR spectra and molecular dynamics studies. *Amino Acids* **2015**, *47*, 2265–2278.
- (76) Rouquet, E.; Roy Chowdhury, M.; Garcia, G. A.; Nahon, L.; Dupont, J.; Lepère, V.; Le Barbu-Debus, K.; Zehnacker, A. Induced photoelectron circular dichroism onto an achiral chromophore. *Nat. Commun.* **2023**, *14*, 6290.
- (77) Fidler, J.; Rodger, P. M.; Rodger, A. Chiral Solvent Structure Around Chiral Molecules: Experimental and Theoretical Study. *J. Am. Chem. Soc.* **1994**, *116*, 7266–7273.
- (78) Wang, S.; Cann, N. M. A molecular dynamics study of chirality transfer: The impact of a chiral solute on an achiral solvent. *J. Chem. Phys.* **2008**, *129*, 054507.
- (79) Konstantinovsky, D.; Perets, E. A.; Santiago, T.; Velarde, L.; Hammes-Schiffer, S.; Yan, E. C. Y. Detecting the First Hydration Shell Structure around Biomolecules at Interfaces. *ACS Cent. Sci.* **2022**, *8*, 1404–1414.
- (80) Mukhopadhyay, P.; Zuber, G.; Wipf, P.; Beratan, D. Contribution of a Solute’s Chiral Solvent Imprint to Optical Rotation. *Angew. Chem. Int. Ed.* **2007**, *46*, 6450–6452.
- (81) Losada, M.; Xu, Y. Chirality transfer through hydrogen-bonding: Experimental and *ab initio* analyses of vibrational circular dichroism spectra of methyl lactate in water. *Phys. Chem. Chem. Phys.* **2007**, *9*, 3127–3135.

- (82) Debie, E.; Jaspers, L.; Bultinck, P.; Herrebout, W.; Van Der Veken, B. Induced solvent chirality: A VCD study of camphor in CDCl₃. *Chem. Phys. Lett.* **2008**, *450*, 426–430.
- (83) Yang, G.; Xu, Y. Probing chiral solute-water hydrogen bonding networks by chirality transfer effects: A vibrational circular dichroism study of glycidol in water. *J. Chem. Phys.* **2009**, *130*, 164506.
- (84) Jähnigen, S.; Sebastiani, D.; Vuilleumier, R. The important role of non-covalent interactions for the vibrational circular dichroism of lactic acid in aqueous solution. *Phys. Chem. Chem. Phys.* **2021**, *23*, 17232–17241.
- (85) Bredehöft, J. H.; Jones, N. C.; Meinert, C.; Evans, A. C.; Hoffmann, S. V.; Meierhenrich, U. J. Understanding Photochirogenesis: Solvent Effects on Circular Dichroism and Anisotropy Spectroscopy. *Chirality* **2014**, *26*, 373–378.
- (86) Eppink, A. T.; Parker, D. H. Velocity map imaging of ions and electrons using electrostatic lenses: Application in photoelectron and photofragment ion imaging of molecular oxygen. *Rev. Sci. Instrum.* **1997**, *68*, 3477–3484.
- (87) Viefhaus, J.; Scholz, F.; Deinert, S.; Glaser, L.; Ilchen, M.; Seltmann, J.; Walter, P.; Siewert, F. The Variable Polarization XUV Beamline P04 at PETRA III: Optics, mechanics and their performance. *Nucl. Instrum. Methods Phys. Res. A* **2013**, *710*, 151–154.

TOC Graphic



Supporting Information: Photoelectron Circular Dichroism of Aqueous-Phase Alanine

Dominik Stemer,^{*,†} Stephan Thürmer,^{*,‡} Florian Trinter,[†] Uwe Hergenhahn,[†]

Michele Pugini,[†] Bruno Credidio,[†] Sebastian Malerz,[¶] Iain Wilkinson,[§]

Laurent Nahon,^{||} Gerard Meijer,[†] Ivan Powis,[⊥] and Bernd Winter^{*,†}

[†]*Fritz-Haber-Institut der Max-Planck-Gesellschaft, Berlin 14195, Germany.*

[‡]*Department of Chemistry, Kyoto University, Kyoto 606-8502, Japan.*

[¶]*Department of Optics and Beamlines, Helmholtz-Zentrum Berlin für Materialien und
Energie, Berlin 14109, Germany.*

[§]*Institute for Electronic Structure Dynamics, Helmholtz-Zentrum Berlin für Materialien
und Energie, Berlin 14109, Germany.*

^{||}*Synchrotron SOLEIL, St. Aubin 91190, France.*

[⊥]*School of Chemistry, The University of Nottingham, Nottingham NG7 2RD, UK.*

E-mail: dstemer@fhi-berlin.mpg.de; thuermer@kuchem.kyoto-u.ac.jp; winter@fhi-berlin.mpg.de

Background Subtraction and Data Analysis

We attempted many approaches to background subtraction, including the use of an experimental background measured for neat water solutions without alanine under the same experimental conditions for which we measured the corresponding alanine spectra. However, we found that such experimentally measured background spectra provided an imperfect fit to the data, and we were unable to sufficiently improve the fit through simple scaling of the spectra. In general, the measurement of an appropriate background spectrum for low-KE PES of condensed-phase targets is not straightforward. Although the simple measurement of a reference sample (e.g. pure water) would seem to provide a reasonable background, the

measured low-energy electron background spectrum of any sample will naturally strongly depend on the integral ionization cross section of all species contained in the sample, their surface propensities, and the specific electron mean free path within that sample. These effects combined to make the measurement of an appropriate experimental background for kinetic energies below 15–20 eV very challenging. We also attempted to measure experimental background spectra by keeping the solution unchanged, and instead increasing the photon energy sufficiently such that the alanine C 1s features were pushed to higher kinetic energy and out of the measurement range. This approach also proved unsuitable, as all of the previously listed factors depend critically on photon energy. Ultimately, we chose to fit the background using a variety of functions and determined that polynomials and sums of polynomials and exponentials constituted the most effective and reproducible background function for these spectra.

Data were analyzed pairwise and for each pair of intensity-corrected spectra, we manually defined a region of interest containing all three of the C 1s peaks and performed a fit to the background with this region masked. We were careful to avoid overfitting, and only accepted a fitted background if small changes to the masked region did not greatly influence the resulting peak shapes and intensities. We then calculated the point-wise difference-over-sum for the + and – data as appears in Eq. 3. This was repeated for the data prior to background subtraction; these data served as a guide during background subtraction and are presented below (Figs. S5, S6, S9, S10, S13, and S14). We identified the peak positions in the background-subtracted data by locating maxima in the second derivatives of the spectra. For each peak, we defined a kinetic-energy window centered at the peak position with a width defined by the full width at half maximum of the peak. Minor differences in peak positions due to offsets in photon energy between left- and right-handed CPL beamline settings were usually less than 5–10 meV and were corrected manually prior to determination of b_1^{+1} . We then calculated the mean and standard deviation for the values of the asymmetry arising from the data within these energy windows. These asymmetries were subsequently multiplied by a geometric factor taking into account the measurement angle of 50° , resulting in a single value of b_1^{+1} per peak based on Eq. 2. This process is illustrated in Fig. S1

A single datapoint, as presented in Fig. S5, thus constitutes the comparison between a pair of spectra measured with left- and right-handed CPL. Each spectrum used for such analysis is in general taken as an average of 10 acquisitions. The time investment for a single data point is approximately one hour of measurement time.

Electronic Circular Dichroism

Absorption-based electronic circular-dichroism measurements were performed using a commercial Chirascan 100 CD spectrophotometer (Applied Photophysics). Dilute (50 mM) aqueous solutions of D-, L-, and DL-alanine were prepared using ultrapure water without pH adjustment, and measured in a quartz cuvette with a 1 mm path length. Electronic circular dichroism spectra were recorded in the wavelength range of 195–250 nm with a step size of 1 nm. For each sample, we measured 3 spectra. The averaged results are presented in Fig. S2

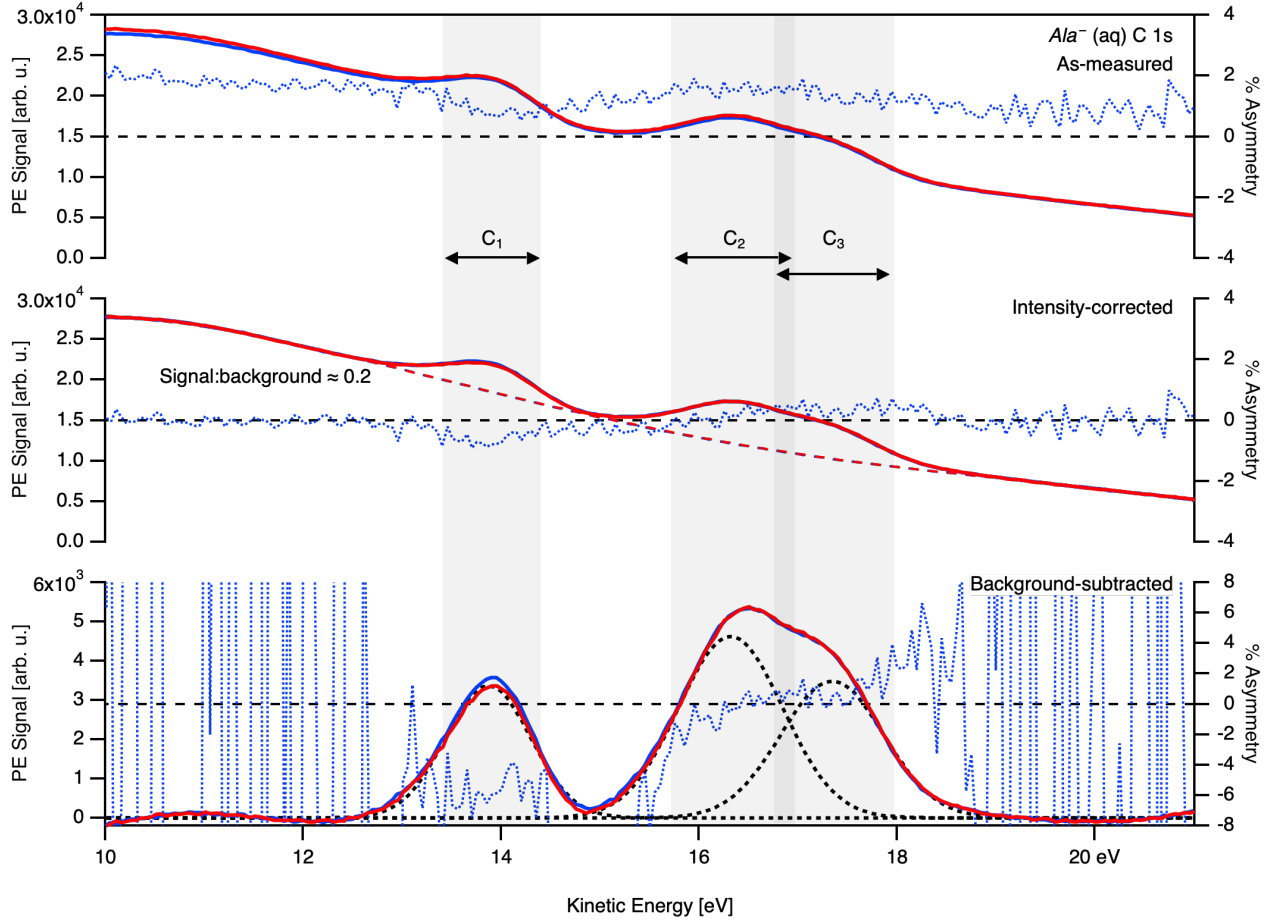


Figure S1: Example of data analysis workflow for a sample pair of spectra measured for Ala^- with $h\nu=307$ eV photons. Top: As-measured spectra measured with left- and right-handed circularly polarized light (blue and red solid lines, respectively), with calculated asymmetry (dotted blue line). Middle: Intensity-corrected spectra and associated background (dashed red and blue lines), with calculated asymmetry. Bottom: Background-subtracted spectra, with associated C1, C2, and C3 peak fits and calculated asymmetry. The gray areas denote the kinetic-energy range within which the asymmetry values are averaged to produce a single value of b_1^{+1} . Note that the magnitude of the asymmetry calculated after background subtraction is significantly larger than that calculated prior to background subtraction, reflecting the low signal-to-background ratio of the as-measured data.

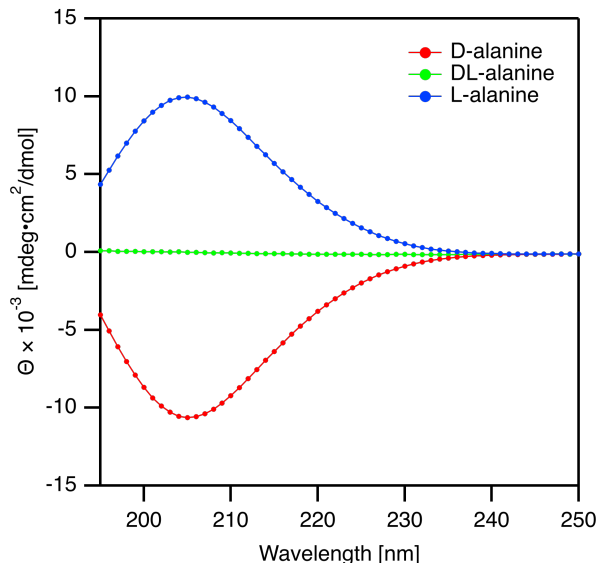


Figure S2: Electronic circular dichroism absorption spectra for 50 mM aqueous solutions of D-, L-, and DL-alanine (red, blue, and green lines, respectively). The data demonstrate clear optical activity only for the enantiopure samples. All data are plotted in units of molar ellipticity.

Calculation of Alanine b_2^0 Photoionization Parameter

Calculations to predict the b_2^0 angular distribution parameter for C 1s photoemission from alanine were made using the CMS- $X\alpha$ method as fully described and applied previously by Tia et al.¹ Those calculations examined the isolated (gas-phase) neutral molecule’s valence photoionization but were here extended to treat core-level photoemission from the three carbon sites. Three different conformers of alanine were modeled, believed to be the most stable configurations of the gas-phase molecule. Conformers 1, 2, and 3 correspond to those descriptions used in reference 1. In the kinetic-energy range investigated, the β parameter for core-level photoionization was found to display little conformer dependence.

Photoelectron Circular Dichroism Data for all Carbon Groups

Although the primary focus of our study was on photoelectron circular dichroism in photoionization of alanine’s COOH/COO⁻ group, we also collected data for alanine’s other carbon centers. Here, we include data corresponding to photoionization of alanine’s chiral center (C₂) and methyl group (C₃), as well as values for b_1^+ based only on the measured data prior to background subtraction.

Error Propagation for Binned Datasets

For clarity, we have displayed the data in the main text following binning of data points using a 250 meV kinetic-energy window. The shaded regions in these plots represent the combined

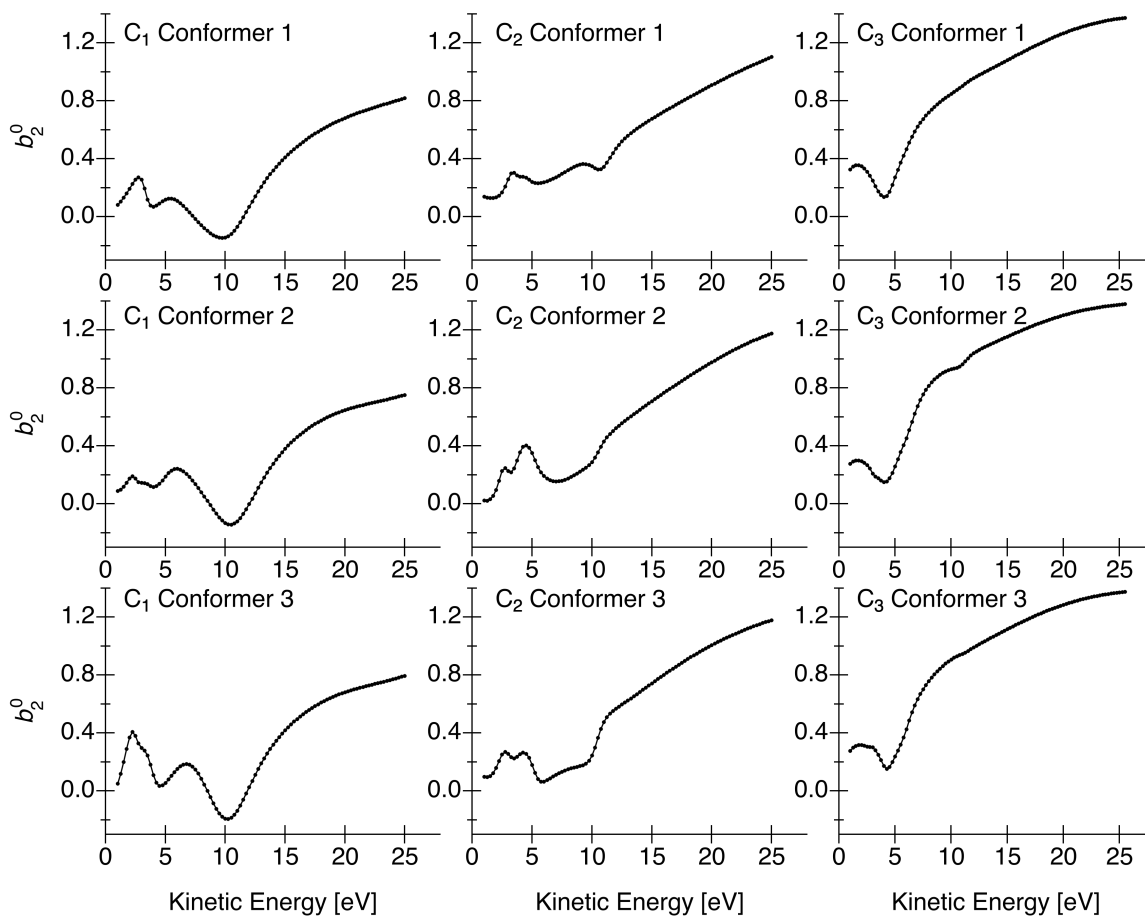


Figure S3: Calculated values of b_2^0 for 1s photoionization of alanine's three carbon groups as a function of photoelectron kinetic energy. C₁, C₂, and C₃ correspond to alanine's carboxylic group, chiral center, and methyl group, respectively, as described in the main text. Conformers 1, 2, and 3 are the same as those discussed in reference 1.

error of the individual data points as well as the spread of the data points binned. The error of each data point was calculated as the standard deviation of the percent difference across the full width at half maximum of the PE feature (see Fig. 3). When n data points were binned together, the error was calculated as:

$$Error = \sqrt{\frac{\sum_{i=1}^n \sigma_i^2}{n^2} + \left(\frac{\sigma_{bin}}{\sqrt{n}}\right)^2}, \quad (1)$$

with σ_i being the error of a given point, and σ_{bin} the standard deviation of the n values of b_1^{+1} in a given bin. The relation propagates the individual error of each data point and the standard error of the mean of all data points within a binning window.

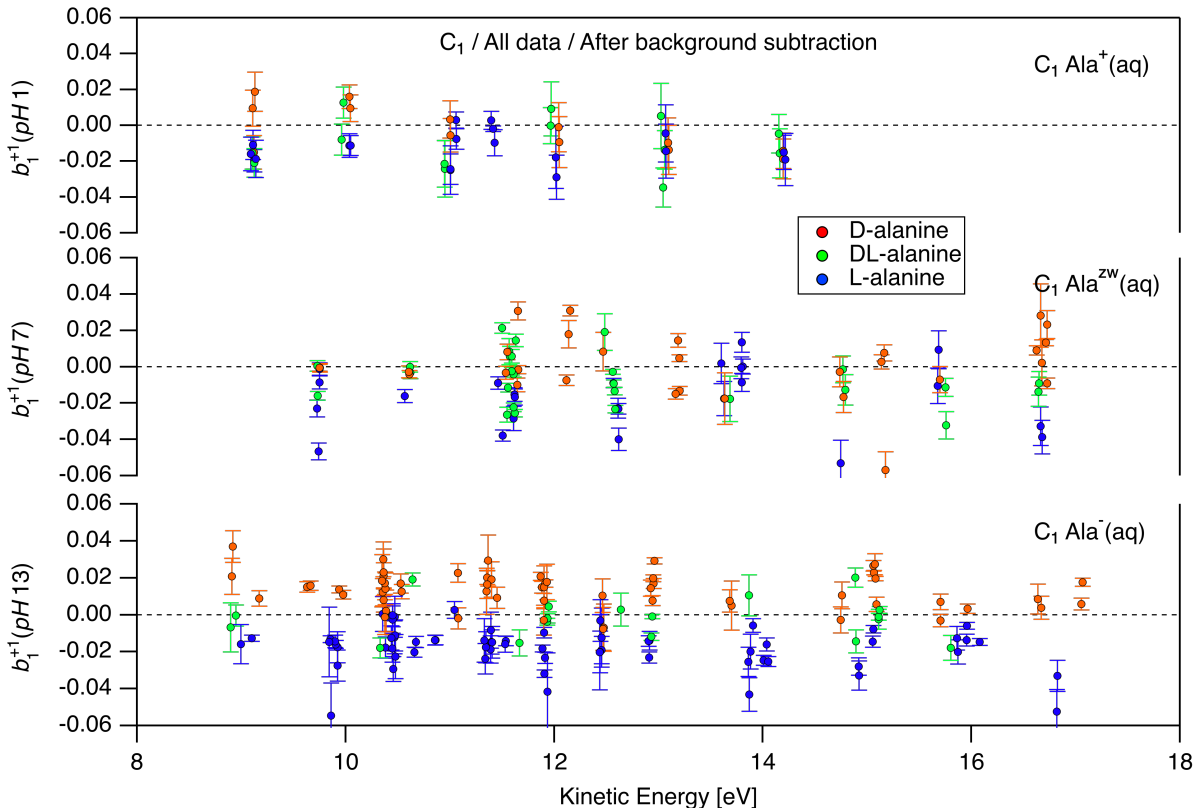


Figure S4: Values of the b_1^{+1} photoionization parameter obtained for C 1s measurements of aqueous solutions of D-, L-, and DL-alanine (red, blue, and green points, respectively) at pH 1, 7, and 13 (top, middle, and bottom; corresponding to the cationic, zwitterionic, and anionic form of the molecule, respectively). All b_1^{+1} values shown correspond to photoionization of the C₁ carboxylic acid group.

References

- (1) Tia, M.; Cunha De Miranda, B.; Daly, S.; Gaie-Levrel, F.; Garcia, G. A.; Nahon, L.; Powis, I. VUV photodynamics and chiral asymmetry in the photoionization of gas phase

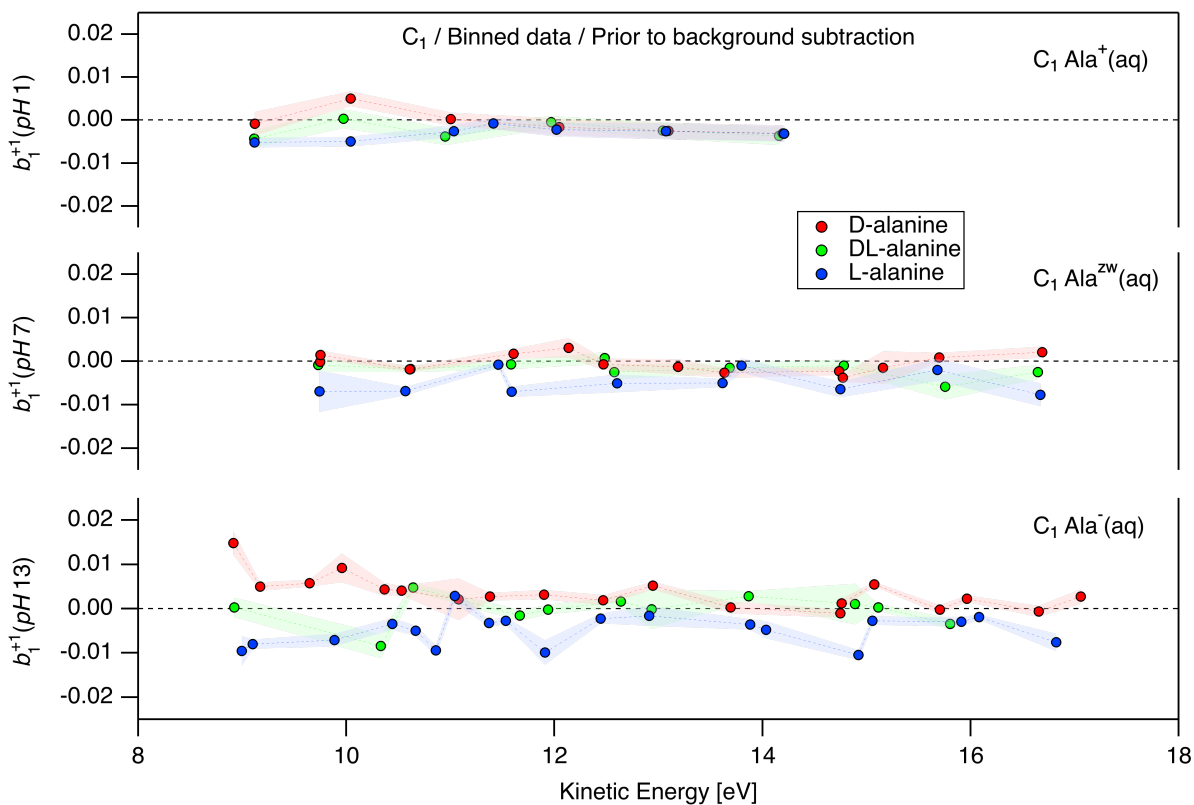


Figure S5: Values of the b_1^{+1} photoionization parameter obtained for C 1s measurements of aqueous solutions of D-, L-, and DL-alanine (red, blue, and green points, respectively) at pH 1, 7, and 13 (top, middle, and bottom; corresponding to the cationic, zwitterionic, and anionic form of the molecule, respectively). All b_1^{+1} values shown correspond to photoionization of the C₁ carboxylic acid group prior to background subtraction. The data is displayed with a kinetic-energy binning of 250 meV.

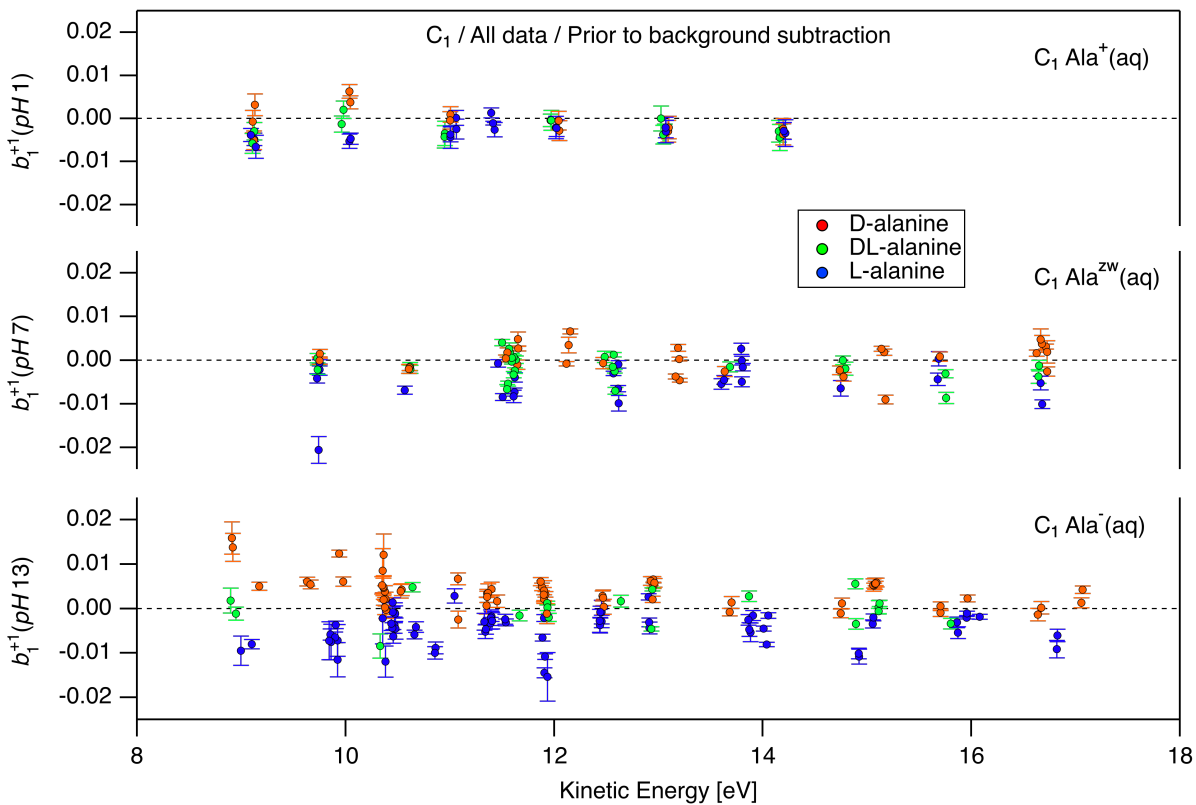


Figure S6: Values of the b_1^{+1} photoionization parameter obtained for C 1s measurements of aqueous solutions of D-, L-, and DL-alanine (red, blue, and green points, respectively) at pH 1, 7, and 13 (top, middle, and bottom; corresponding to the cationic, zwitterionic, and anionic form of the molecule, respectively). All b_1^{+1} values shown correspond to photoionization of the C₁ carboxylic acid group prior to background subtraction.

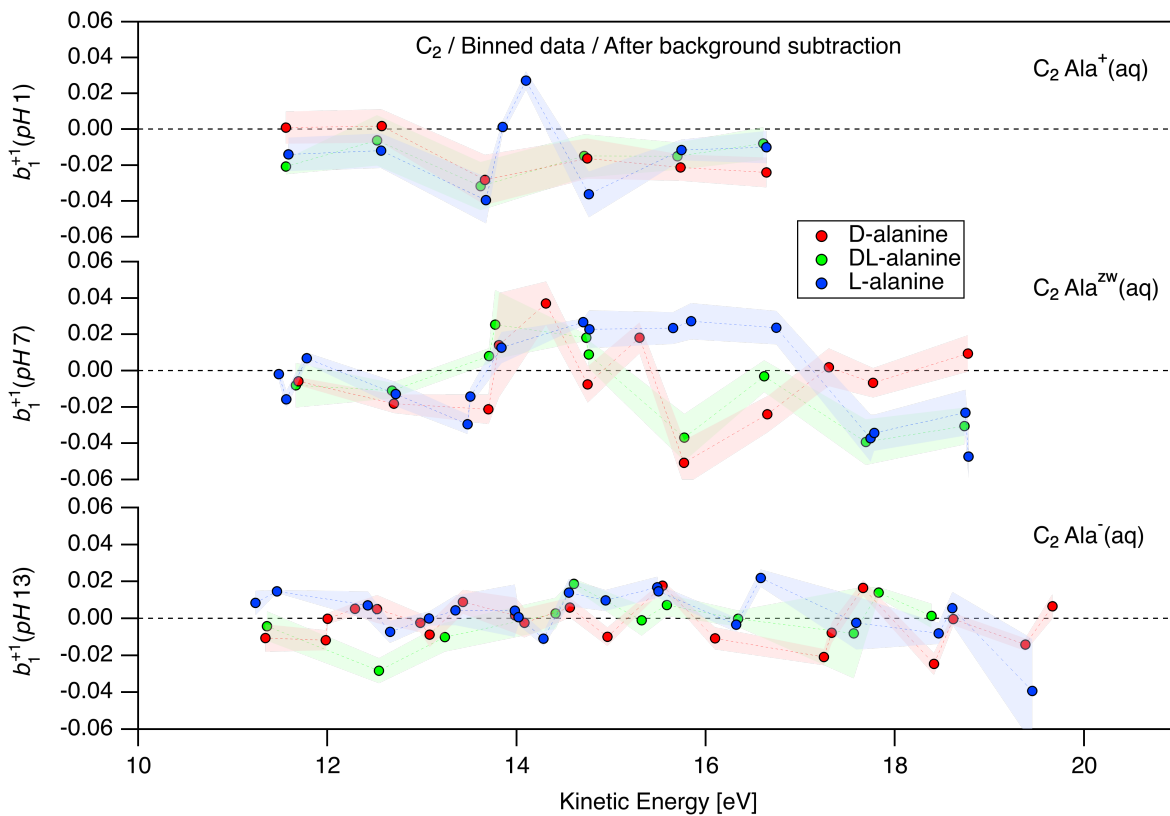


Figure S7: Values of the b_1^{+1} photoionization parameter obtained for C 1s measurements of aqueous solutions of D-, L-, and DL-alanine (red, blue, and green points, respectively) at pH 1, 7, and 13 (top, middle, and bottom; corresponding to the cationic, zwitterionic, and anionic form of the molecule, respectively). All b_1^{+1} values shown correspond to photoionization of the C₂ chiral center. The data is displayed with a kinetic-energy binning of 250 meV.

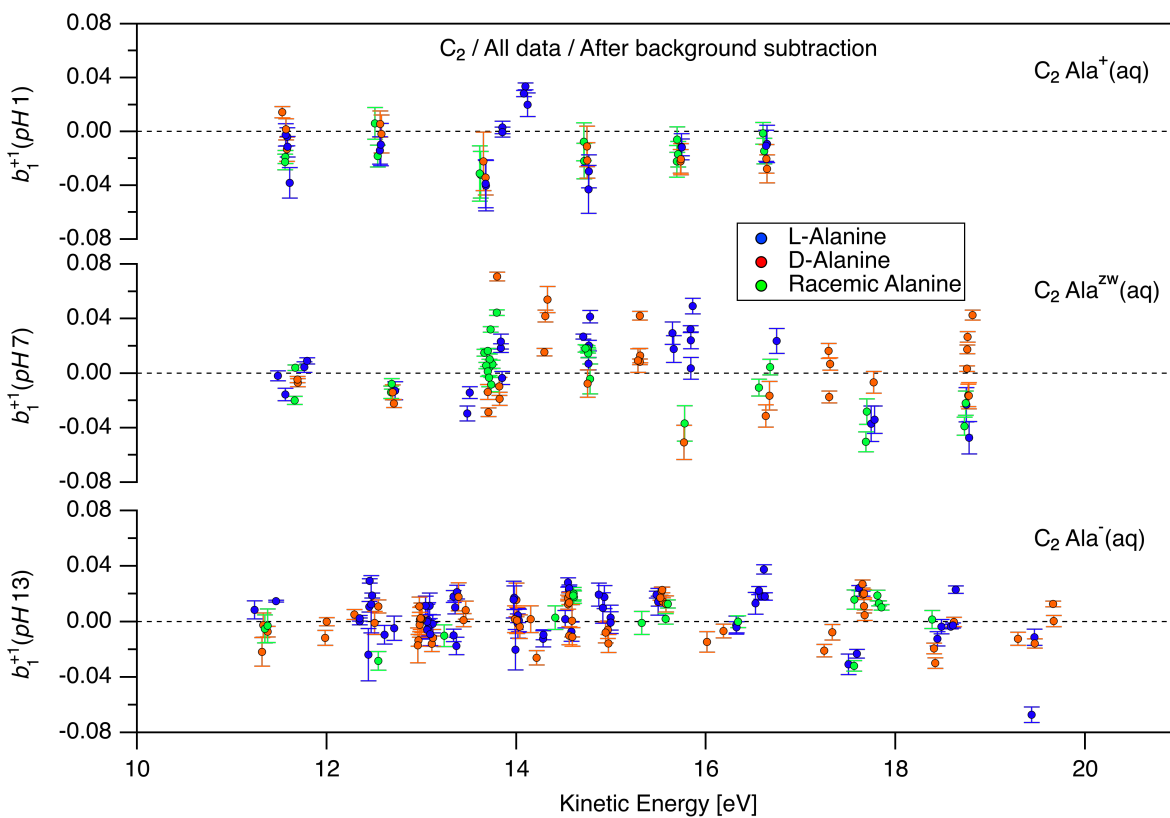


Figure S8: Values of the b_1^{+1} photoionization parameter obtained for C 1s measurements of aqueous solutions of D-, L-, and DL-alanine (red, blue, and green points, respectively) at pH 1, 7, and 13 (top, middle, and bottom; corresponding to the cationic, zwitterionic, and anionic form of the molecule, respectively). All b_1^{+1} values shown correspond to photoionization of the C_2 chiral center.

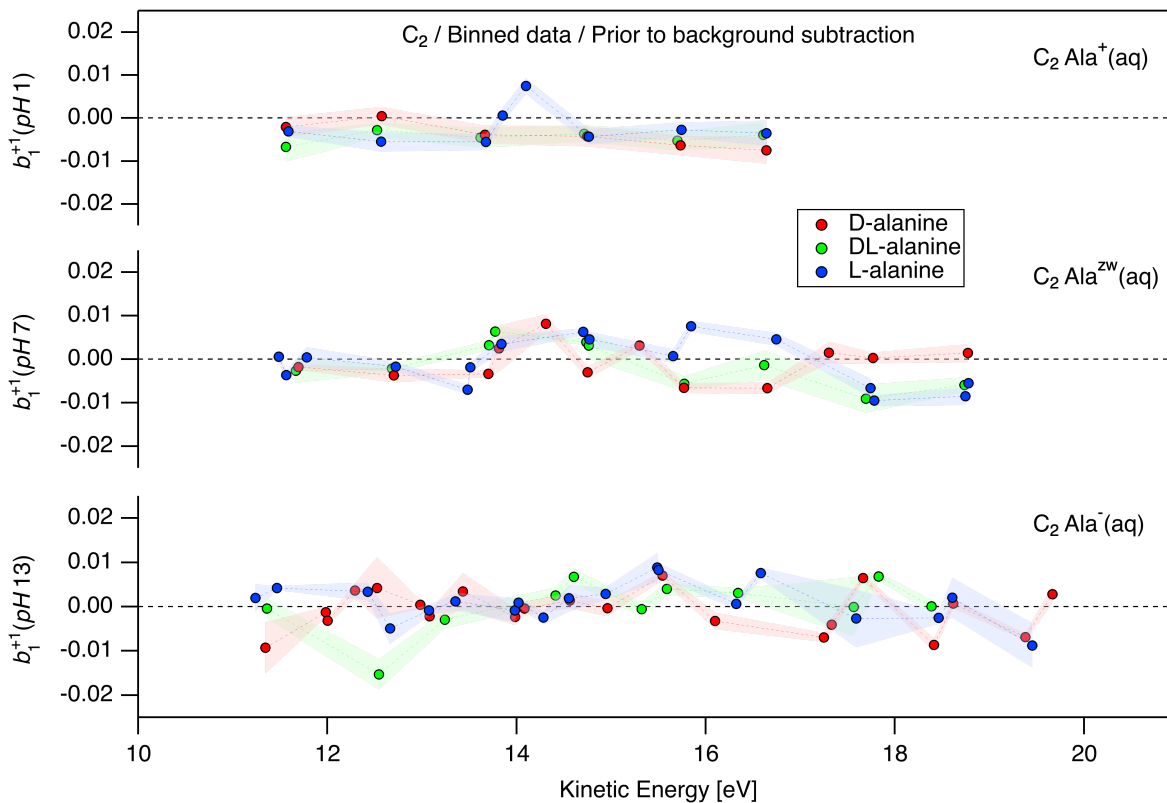


Figure S9: Values of the b_1^{+1} photoionization parameter obtained for C 1s measurements of aqueous solutions of D-, L-, and DL-alanine (red, blue, and green points, respectively) at pH 1, 7, and 13 (top, middle, and bottom; corresponding to the cationic, zwitterionic, and anionic form of the molecule, respectively). All b_1^{+1} values shown correspond to photoionization of the C₂ chiral center prior to background subtraction. The data is displayed with a kinetic-energy binning of 250 meV.

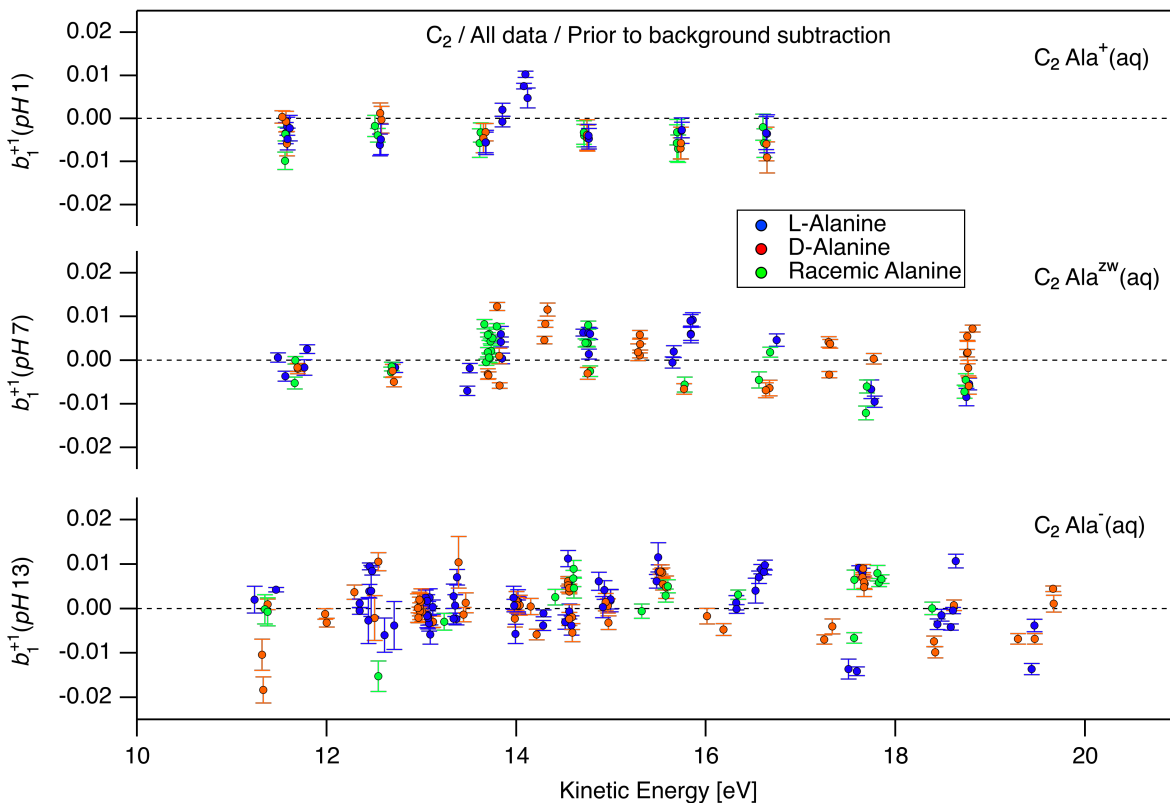


Figure S10: Values of the b_1^{+1} photoionization parameter obtained for C 1s measurements of aqueous solutions of D-, L-, and DL-alanine (red, blue, and green points, respectively) at pH 1, 7, and 13 (top, middle, and bottom; corresponding to the cationic, zwitterionic, and anionic form of the molecule, respectively). All b_1^{+1} values shown correspond to photoionization of the C₂ chiral center prior to background subtraction.

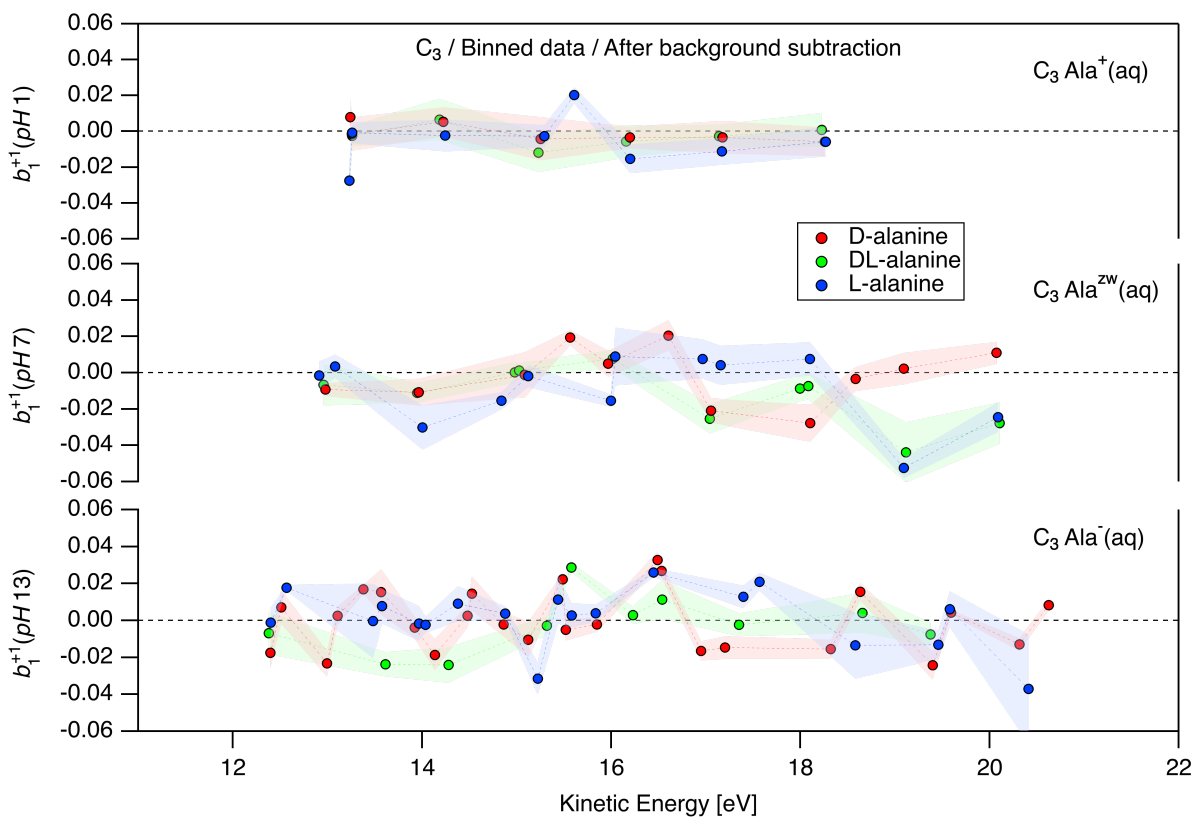


Figure S11: Values of the b_1^{+1} photoionization parameter obtained for C 1s measurements of aqueous solutions of D-, L-, and DL-alanine (red, blue, and green points, respectively) at pH 1, 7, and 13 (top, middle, and bottom; corresponding to the cationic, zwitterionic, and anionic form of the molecule, respectively). All b_1^{+1} values shown correspond to photoionization of the C₃ methyl group. The data is displayed with a kinetic-energy binning of 250 meV.

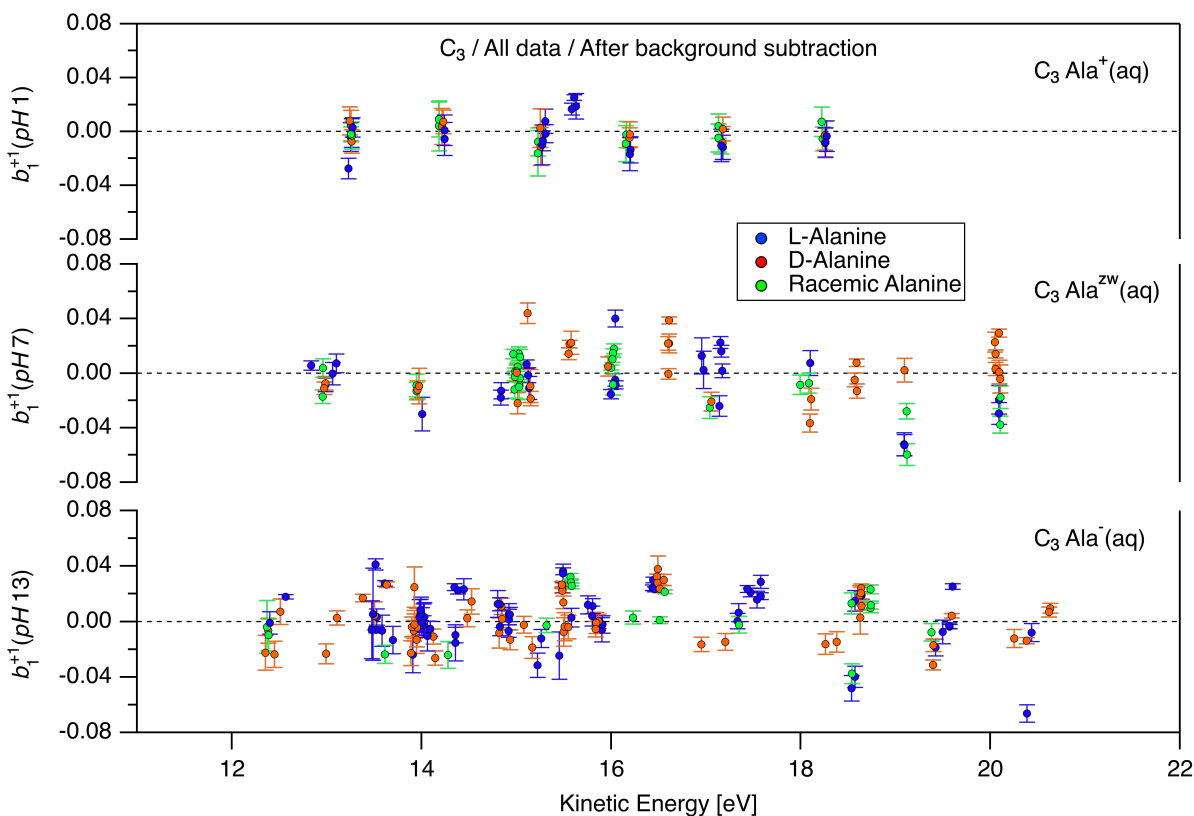


Figure S12: Values of the b_1^{+1} photoionization parameter obtained for C 1s measurements of aqueous solutions of D-, L-, and DL-alanine (red, blue, and green points, respectively) at pH 1, 7, and 13 (top, middle, and bottom; corresponding to the cationic, zwitterionic, and anionic form of the molecule, respectively). All b_1^{+1} values shown correspond to photoionization of the C₃ methyl group.

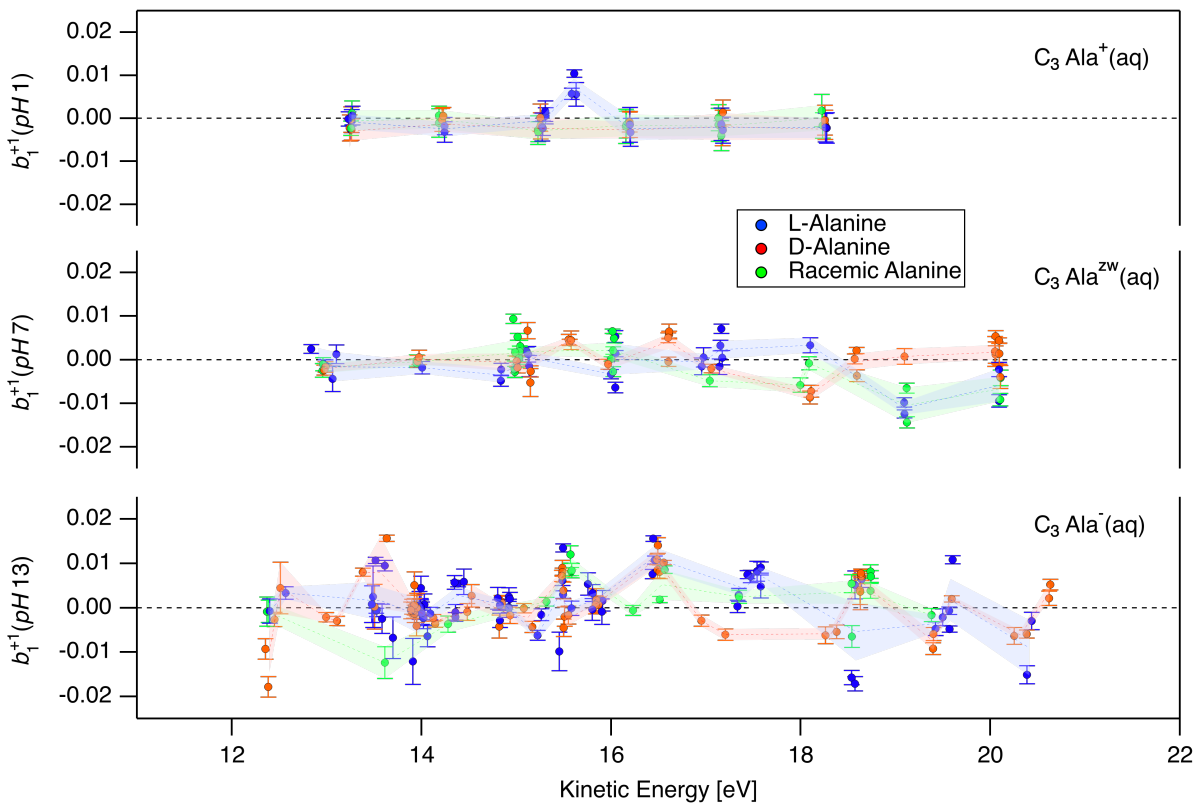


Figure S13: Values of the b_1^{+1} photoionization parameter obtained for C 1s measurements of aqueous solutions of D-, L-, and DL-alanine (red, blue, and green points, respectively) at pH 1, 7, and 13 (top, middle, and bottom; corresponding to the cationic, zwitterionic, and anionic form of the molecule, respectively). All b_1^{+1} values shown correspond to photoionization of the C_3 methyl group prior to background subtraction. The data is displayed with a kinetic-energy binning of 250 meV.

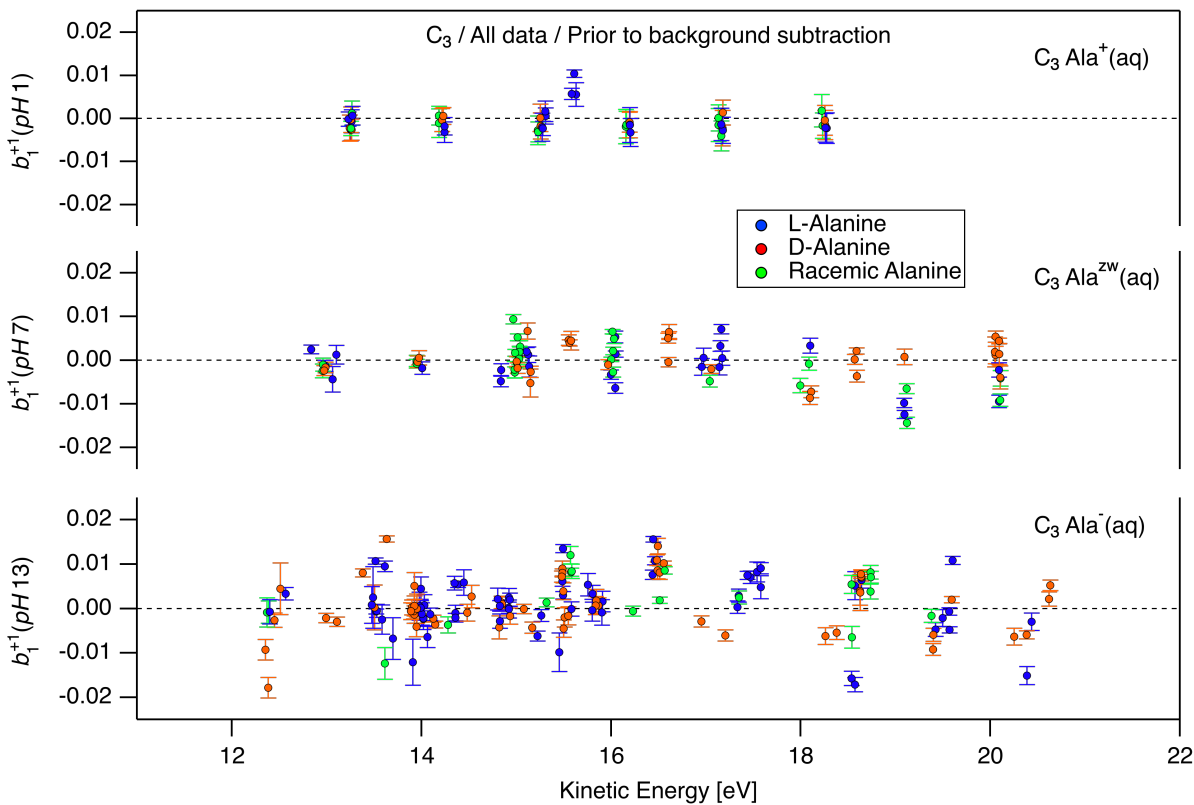


Figure S14: Values of the b_1^{+1} photoionization parameter obtained for C 1s measurements of aqueous solutions of D-, L-, and DL-alanine (red, blue, and green points, respectively) at pH 1, 7, and 13 (top, middle, and bottom; corresponding to the cationic, zwitterionic, and anionic form of the molecule, respectively). All b_1^{+1} values shown correspond to photoionization of the C_3 methyl group prior to background subtraction.

alanine enantiomers. *J. Phys. Chem. A* **2014**, *118*, 2765–2779.